Paleoceanography and Paleoclimatology

RESEARCH ARTICLE
10.1029/2018PA003363

Key Points:
- Productivity is highest during interglacial periods
- Productivity varies in step with global climate
- Glacial stratification may be driven by a strong pycnocline, weak winds, and/or reduced subsurface nutrient concentrations

Supporting Information:
- Supporting Information S1
- Table S1
- Table S2
- Table S3

Correspondence to:
K. M. Costa,
kcosta@ldeo.columbia.edu

Citation:
Costa, K. M., McManus, J. F., & Anderson, R. F. (2018). Paleoproductivity and stratification across the Subarctic Pacific over glacial-interglacial cycles. *Paleoceanography and Paleoclimatology*, *33*. https://doi.org/ 10.1029/2018PA003363

Received 13 MAR 2018
Accepted 1 AUG 2018
Accepted article online 9 AUG 2018

Paleoproductivity and Stratification Across the Subarctic Pacific Over Glacial-Interglacial Cycles

Kassandra M. Costa[1,2], Jerry F. McManus[1,2], and Robert F. Anderson[1,2]

[1]Lamont-Doherty Earth Observatory, Columbia University, Palisades, NY, USA, [2]Department of Earth and Environmental Sciences, Columbia University, New York, NY, USA

Abstract In the Subarctic Pacific, variability in productivity on glacial-interglacial timescales is often attributed to changes in stratification and nutrient delivery to the surface, but the mechanisms driving this relationship are poorly constrained. Records extending beyond the last glacial maximum from both the open ocean and the marginal seas are required to investigate the timing and magnitude of different influential processes through the full glacial cycle. In this study we generated $^{231}Pa/^{230}Th$ over 210,000 years in order to capture two full glacial cycles of paleoproductivity on the Juan de Fuca Ridge in the East Subarctic Pacific. The sedimentary $^{231}Pa/^{230}Th$ ratios are always equal to or greater than the seawater production ratio (0.093), consistent with enhanced biological scavenging in this region. The temporal pattern of $^{231}Pa/^{230}Th$ burial is remarkably coherent with changes in climate, with high values (0.20) during peak interglacial periods descending to low values (0.10) during peak glacial conditions, consistent with other long productivity records from this region. We investigate the possible contributions of temperature, sea ice formation, Bering Strait closure, wind strength, upwelling, and subsurface nutrient concentrations as possible mechanisms by which physical and/or chemical stratification emerged during glacial periods. Due to the low sea surface salinity in the North Pacific, cooling actually weakens the density gradient in surface (0–200 m) waters. To create the steep density profiles that characterize physical stratification, additional processes to reduce the salinity of surface waters must occur during glacial periods. We suggest that regional sea ice formation and Bering Strait closure may have contributed to freshening surface waters and enhancing physical stratification during glacial periods. Additionally, simulated weak winds in this region due to the southward shift of the glacial westerlies may have further reduced surface mixing depths in the Subarctic Pacific. Finally, previous model simulations suggest strong glacial wind stress curl in the Subarctic Pacific, but enhanced Ekman divergence of nutrient-poor subsurface waters would have little impact on stimulating productivity in surface waters of the Subarctic Pacific. We therefore suggest that the combined effects of surface freshening, weak winds, and lower subsurface nutrient concentrations may all have contributed to lower productivity during glacial periods in the Subarctic Pacific.

1. Introduction

Productivity in the Subarctic Pacific is sensitive to light and nutrient limitation controlled by the physical processes of stratification, winter mixing, and sea ice formation. At the onset of Northern Hemisphere glaciation (2.7Ma), the development of a steep halocline created a permanent shift toward greater physical stratification and lower baseline productivity (Haug et al., 1999). During the last deglaciation, abrupt and transient climate events stimulated productivity peaks at the Bolling-Allerod (Addison et al., 2012; Cook et al., 2005; Davies et al., 2011; Gebhardt et al., 2008; Gorbarenko et al., 2004; Hendy & Cosma, 2008; Kohfeld & Chase, 2011; Lam et al., 2013; Ren et al., 2015), for a variety of proposed mechanisms related to, for example, meltwater pulses, iron fertilization, subsurface nutrient concentrations, and vertical mixing. Yet neither million year nor millennial mechanisms are directly analogous to those of glacial-interglacial variability in productivity, which arises from a gradual transition to a semipermanent glacial state that lasts for tens of thousands of years. Glacial-interglacial changes in productivity are often attributed to greater physical and/or chemical stratification that reduced nutrient delivery to surface waters during glacial periods (Brunelle et al., 2007, 2010; Galbraith et al., 2008; Jaccard et al., 2005; Kienast et al., 2004; Knudson & Ravelo, 2015a; Narita et al., 2002; Sigman et al., 2004), but the mechanism(s) by which these stable conditions develop and persist on orbital timescales remain elusive.

In this study, we generate new records of productivity ($^{231}Pa/^{230}Th$, opal flux, and excess silica flux) from the East Subarctic Pacific (approximately 45°N, 230°E, 2,700 m) over the last two glacial cycles. Disagreement between various productivity proxies is not uncommon and may lead to ambiguous paleo-productivity trends (e.g., in the equatorial Pacific; Anderson & Winckler, 2005; Costa et al., 2017), and in the Subarctic (Costa et al., 2018; Serno et al., 2014). Because $^{231}Pa/^{230}Th$ is the productivity proxy least susceptible to pre- servation biases, it may provide the most reliable reconstruction of paleoproductivity while allowing the qua- litative assessment of the impact of preservation and diagenesis on other proxies, particularly opal, in the Subarctic Pacific. Compiling this new record with other long productivity records from across the region, including the Okhotsk Sea (Brunelle et al., 2010; Gorbarenko et al., 2004; Sato et al., 2002), Bering Sea (Brunelle et al., 2007; Knudson & Ravelo, 2015a; Riethdorf et al., 2013), West Subarctic (Brunelle et al., 2010; Jaccard et al., 2009; Shigemitsu et al., 2007), and East Subarctic (Kienast, 2003; McDonald et al., 1999), allows for the distinction of both spatial and temporal patterns that may help to identify or eliminate possible mechanisms for increased stratification during glacial periods (Kienast et al., 2004). We consider the roles of temperature change, sea ice formation, Bering Strait closure, wind strength, upwelling rates, and subsur- face nutrient concentrations as potential processes contributing to variability in stratification and productiv- ity over glacial-interglacial periods.

2. Theoretical Framework and Analytical Methodology

2.1. Scavenging of ^{230}Th and ^{231}Pa in the Water Column

^{230}Th is produced in the water column by ^{238}U decay (β = 0.02556 dpm/m^3 year, at salinity of 35), and it is rapidly removed from the water column by adsorption onto settling particles, in a process referred to as scavenging. Uranium decay to ^{230}Th is spatially constant due to the high solubility and long residence time (400 kyr) of uranium, which results in a fairly constant uranium concentration (3.2 ppb) that scales conserva- tively with salinity (Owens et al., 2011). The uncertainty introduced by using a constant production rate is small ($<$5%), both spatially, because salinity varies little in the deep ocean where most ^{230}Th is produced, and temporally, because glacial-interglacial changes in salinity are offset by changes in sea level.
Therefore, the ^{230}Th flux to the sediment is primarily dependent on the water column depth over which the sediment integrates (Henderson & Anderson, 2003), and its sedimentary concentrations are inversely pro- portional to the flux of sediment with which the ^{230}Th is diluted (Francois et al., 2004). The residence time of ^{230}Th in the ocean is so short (20–40 years; Nozaki et al., 1981) compared to its half-life (75,584 years; Cheng et al., 2013) that virtually all of the ^{230}Th produced by uranium decay in seawater is removed to sediments by scavenging in the water column. The residence time of ^{230}Th is also much less than the time scale for lateral transport by mixing from regions of low scavenging intensity (low particle flux) to regions of high scavenging intensity. Consequently, most ^{230}Th is buried in sediment underlying the very same water column in which it was produced (Henderson et al., 1999; Henderson & Anderson, 2003).

^{231}Pa, like ^{230}Th, is produced by uranium (^{235}U) decay (β = 0.00245 dpm/m^3 year, at salinity of 35) in the water column and scavenged by particles settling to the seafloor, but unlike ^{230}Th, ^{231}Pa has a residence time long enough to advect and diffuse away from the water column in which it was produced. Scavenging of ^{231}Pa from the water column is much less effective, and it can be dependent on both the particle flux (Anderson et al., 1983, 1990; Bacon, 1988; Hayes et al., 2013) and the particle composition (Chase et al., 2002, 2003; Geibert & Usbeck, 2004; Kretschmer et al., 2011). In regions with low particle flux, more ^{231}Pa will escape local scavenging, and particles will likely acquire a $^{231}Pa/^{230}Th$ much lower than that of production in the water column ($\beta_{231Pa}/\beta_{230Th}$ = 0.093; activity ratio, at salinity of 35). In regions of high particle flux, in situ and allochthonous ^{231}Pa will be more efficiently scavenged so that particles acquire high $^{231}Pa/^{230}Th$, potentially greater than production. Similarly, opal has a particular affinity for ^{231}Pa, so that opal rich sediments will tend to have relatively high ^{231}Pa concentrations and thus $^{231}Pa/^{230}Th$ greater than production ($^{231}Pa/^{230}Th > 0.093$). The lateral mobility of ^{231}Pa relative to ^{230}Th generates sedimentary $^{231}Pa/^{230}Th$ unequal to the production ratio over much of the ocean (Hayes et al., 2014), with the high $^{231}Pa/^{230}Th$ con- centrated in a limited zone along continental margins (Figure 1). These high $^{231}Pa/^{230}Th$ are generated at continental boundaries because terrigenous inputs, coastal upwelling, and high productivity combine to generate high particle and opal fluxes, and so the major removal process of ^{231}Pa in these settings is known as boundary scavenging (Anderson et al., 1983, 1990; Bacon, 1988; Hayes et al., 2013).

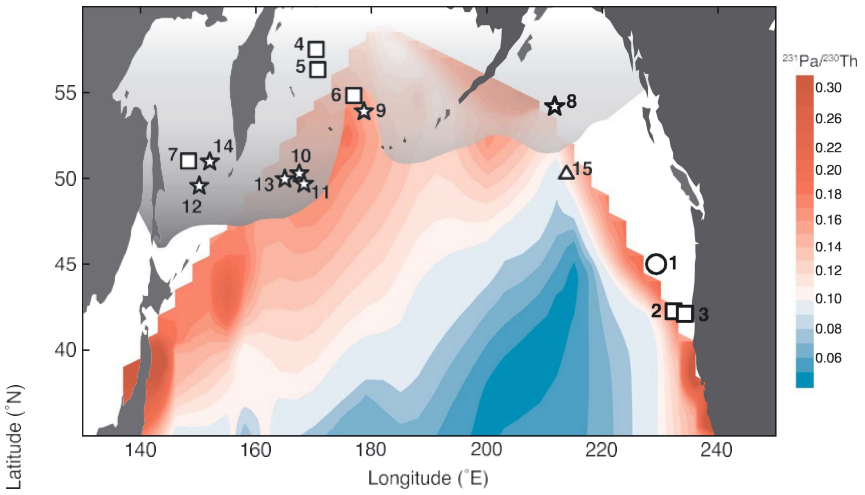

Figure 1. Distribution of coretop $^{231}Pa/^{230}Th$ in the North Pacific. Compiled by Hayes et al. (2014). $^{231}Pa/^{230}Th$ follows modern productivity patterns, with low values (below production, 0.093 activity ratio) characterizing the gyre and high values (above production) characterizing the continental margins. The white circle (1) identifies the location of the Juan de Fuca Ridge. Squares indicate long (>60 kyr) productivity records based on organic carbon: (2) W8709-8 and (3) W8709-13 (Kienast, 2003), (4) SO201-2-85 and (5) SO201-2-77 (Riethdorf, Nurnberg, et al., 2013), (6) U1342 (Knudson & Ravelo, 2015a), and (7) PC936 (Gorbarenko et al., 2004). Stars indicate long productivity records based on excess barium: (8) ODP887 (McDonald et al., 1999), (9) JPC17 (Brunelle et al., 2007), (10) ODP882 (Jaccard et al., 2009), (11) RNDP-PC13 and (12) GGC27 (Brunelle et al., 2010), (13) MR98-05-3PC (Shigemitsu et al., 2007), and (14) X98-01PC (Sato et al., 2002). See Table 1 for site locations. Ocean Station PAPA (15) is shown as a triangle. Gray shaded area indicates the maximum seasonal sea ice extent during the LGM, based on reconstructions from diatom assemblages, ice rafted debris, and IP_{25} (Matul, 2017; Méheust et al., 2018).

2.2. Materials and Methods

Sediment cores were collected from the Juan de Fuca Ridge (JdFR) on the SeaVOICE cruise (AT26-19) of the R/V Atlantis in September 2014 (Table 1). The cores are closely clustered (within 50 km) and from similar depth range (2,655–2,794 m), such that they can be combined as if multiple iterations of the same paleorecord (e.g., Costa & McManus, 2017). Age models for the JdFR piston cores are well constrained based on radiocarbon dates, benthic $\delta^{18}O$, and stratigraphically tuned density cycles (Costa et al., 2017). Additionally, two multicores (06MC and 10MC) corresponding to piston cores (09PC and 12TC/PC respec- tively) are added to cover the Holocene. Age models for these multicores are primarily based on benthic $\delta^{18}O$ due to bioturbative effects on core top radiocarbon dates (Costa, McManus, & Anderson, 2017). Sedimentation rates over the past 500 kyr generally range from 1 to 3 cm/kyr, with background pelagic sedimentation rates close to 1 cm/kyr, and they are spatially heterogeneous, likely reflecting sediment remobilization caused by the high relief and stronger bottom currents of the near-ridge environment (Costa et al., 2016).

2.2.1. Uranium Series Chemistry

A total of 520 samples were analyzed for thorium (^{230}Th and ^{232}Th), uranium (^{238}U, ^{235}U, and ^{234}U), and protactinium (^{231}Pa) by isotope dilution using inductively coupled plasma mass spectrometry (ICP-MS). Data for ^{230}Th have been previously published by Costa and McManus (2017), and ^{231}Pa data were ana- lyzed by a similar methodology. Samples (100 mg) were spiked with ^{233}Pa and processed with complete acid digestion and column chromatography (Fleisher & Anderson, 2003). Isotopes were measured on an Element 2 ICP-MS at the Lamont-Doherty Earth Observatory of Columbia University. Discrete sediment ali- quots (n = 40) of the VOICE Internal Mega-Standard (VIMS; Costa & McManus, 2017) were processed and analyzed for quality control, and these total replicates of VIMS indicate that the analytical procedure and measurement are externally reproducible within 8.7% on ^{231}Pa. Excess initial ^{231}Pa ($^{231}Pa_{xs}{}^{0}$) concentra- tions were calculated by correcting for supported decay from lithogenic and authigenic uranium (Henderson & Anderson, 2003). Throughout this text, $^{231}Pa/^{230}Th$ will refer specifically to the excess initial isotope ratio, corrected for radioactive decay since deposition. Data are provided in supporting informa- tion Table S1.

Table 1
Core Locations Used in This Study

Region	Core	Lat °N	Long °E	Water depth (m)	Average Sedimentation rate (cm/kyr)	Proxy	Reference
East Subarctic	AT26-19-05PC	44.973	229.122	2711	0.93	$^{231}Pa/^{230}Th$	this study
East Subarctic	AT26-19-09PC/06MC	44.887	229.363	2678	1.95	$^{231}Pa/^{230}Th$	this study
East Subarctic	AT26-19-12PC-TC/ 10MC	44.898	229.496	2689	0.63	$^{231}Pa/^{230}Th$	this study
East Subarctic	AT26-19-35PC	44.991	229.543	2731	1.85	$^{231}Pa/^{230}Th$	this study
East Subarctic	AT26-19-38PC	44.971	229.393	2655	1.11	$^{231}Pa/^{230}Th$	this study
East Subarctic	AT26-19-39BB	45.045	229.167	2794	1.18	$^{231}Pa/^{230}Th$	this study
East Subarctic	W8709A-8	42.270	232.320	3111	9.49	Organic C	Kienast (2003)
East Subarctic	W8709A-13	42.120	234.250	2712	14.11	Organic C	Kienast (2003)
West Subarctic	ODP882	50.330	167.500	3244	6.03	Biogenic Ba	Jaccard et al. (2009)
East Subarctic	ODP887	54.220	211.730	3647	7.08	Biogenic Ba	McDonald et al. (1999)
West Subarctic	RNDP-PC-13	49.720	168.300	2393	4.33	Biogenic Ba	Brunelle et al. (2010)
Okhotsk Sea	GGC27	49.601	150.180	995	2.52	Biogenic Ba	Brunelle et al. (2010)
Bering Sea	JPC17	53.933	178.699	2209	12.90	Biogenic Ba	Brunelle et al. (2007)
Bering Sea	U1342	54.828	176.917	818	3.65	Organic C	Knudson and Ravelo (2015a)
Okhotsk Sea	PC936	51.015	148.313	1305	5.35	Organic C	Gorbarenko et al. (2004)
West Subarctic	MR98-05-3PC	50.000	164.983	5507	3.59	Biogenic Ba	Shigemitsu et al. (2007)
Okhotsk Sea	X98-01PC	51.015	152.008	1100	8.11	Biogenic Ba	Sato et al. (2002)
Bering Sea	SO201-2-85	57.505	170.413	975	10.67	Organic C	Riethdorf, Nurnberg, et al. (2013)
Bering Sea	SO201-2-77	56.330	170.699	2133	9.49	Organic C	Riethdorf, Nurnberg, et al. (2013)

2.2.2. Opal and Excess Silica Fluxes

Biogenic opal was measured by alkaline extraction (Mortlock & Froelich, 1989) at LDEO and has been previously published (Costa et al., 2018). Total replicates (n = 6) of VIMS indicate that the analytical procedure and measurement are reproducible within ±6.7%.

Total silica and titanium concentrations were analyzed by flux fusion following the procedure of Murray et al. (2000). Dried, homogenized samples (100 ± 5 mg) were combined with lithium metaborate flux (400 ± 10 mg) in graphite crucibles and fused at 1050°C for 8–10 min. The graphite crucibles were removed from the furnace and agitated to ensure aggregation of the fused material. After reheating to 1050°C, the fused bead was dissolved in 10% HNO_3, agitated for approximately 10 min, and then filtered and diluted for analysis. Samples were analyzed on an Agilent 720 ICP optical emission spectrometer at LDEO, and ICP optical emis- sion spectrometer intensity data were calibrated to concentrations with fluxed standard reference materials (JLS-1, JDO-1, SCO-1, AGV-2, JB1-a, W-2a, BCR, and BHVO-2). Total replicates (n = 10) of VIMS indicate that the analytical procedure and measurement are reproducible within ±2.8% for Si and ±1.8% for Ti.

Total silica concentrations comprise both terrigenous silica and biogenic (or excess) silica. To isolate the excess silica (Si_{xs}) fraction, the terrigenous silica is estimated using titanium concentrations and a constant lithogenic Si/Ti ratio. Bulk continental crust has a Si/Ti of 49.6 wt%/wt% (Taylor & McLennan, 1995), but the slightly lower value of 47 wt%/wt% was used here to eliminate negative results. In summary

$$[Si_{xs}] = [Si_{total}] - [Ti] \times \left(\frac{Si}{T}\right)_{Lit}$$

Opal and Si_{xs} data are provided in supporting information Table S2.

2.2.3. Data Compilation

This study focuses on paleoproductivity changes on glacial-interglacial timescales, and thus, it requires long productivity proxy records that extend beyond the last glacial maximum (Table 1). The criteria for inclusion in this study were (1) at least the last 60 kyr of continuous data coverage, (2) data available on major sedimentary components ($CaCO_3$, opal) to correct for dilution effects, and (3) location in the Subarctic Pacific above 40°N. Age models used in this study have not been changed from their originally published values.

Ideally, productivity proxies would be normalized to a constant flux proxy (CFP), like ^{230}Th or ^{3}He, which can be used to calculate the absolute flux of a sedimentary component over time (Francois et al., 2004). Unfortunately, many productivity proxy records are published without CFP normalization, and they are instead presented as age-model-based mass accumulation rates or simply as concentrations. Compared to

CFP derived fluxes, age-model-based mass accumulation rates are notoriously inaccurate (see discussion in Costa & McManus, 2017; Francois et al., 2004; Kienast et al., 2007; Winckler et al., 2016), due to omnipresent lateral sediment redistribution on the seafloor. Because using these mass accumulation rates can cause misleading interpretations (e.g., Murray et al., 2012 compared to Winckler et al., 2016), we do not employ them for any of the proxy records in this study.

Instead, we use proxy concentration data that have been corrected for dilution by variability in major sedimentary components, specifically calcium carbonate and opal. Calcium carbonate preservation in the Pacific varies on glacial-interglacial timescales such that calcium carbonate burial is higher during glacial per- iods than interglacial periods (e.g., Farrell & Prell, 1989). An increase in the relative concentration (wt%) of, for example, organic carbon may be due to increased productivity, but it could just as easily result from a decreased concentration of calcium carbonate. The dilution correction is calculated by determining the proxy concentration on a calcium carbonate (and opal) free basis (e.g., Bonatti et al., 1971; Bostrom & Peterson, 1966; Karlin et al., 1987) as follows:

$$\left(\text{Proxy}\right)_{\text{Proxy}} \frac{100}{100 - [\%\text{CaCO}_3] - [\%\text{Opal}]}$$

where the proxy of interest may be organic carbon or excess barium concentrations. We focus on minor sedimentary constituents rather than major constituents, like opal, which may be more sensitive to preservation effects (as discussed later in section 4.1). Corrections were made for both calcium carbonate and opal where available, with the largest effects due to calcium carbonate in the Subarctic Ocean and opal in the Okhotsk and Bering Seas. Previous studies reach similar conclusions based on ^{230}Th-normalized elemental fluxes and elemental concentrations on a carbonate-free basis (Costa et al., 2018). Corrected and uncorrected data are provided in supporting information Table S3.

3. Results

^{231}Pa/^{230}Th from the six sites on the Juan de Fuca Ridge show similar glacial-interglacial trends (Figure 2). The ratios are generally high during interglacial periods and low during glacial periods, with a temporal evolution that mimics the sawtooth pattern of a climate record (e.g., benthic δ^{18}O; Lisiecki & Raymo, 2005). Throughout the last 200 kyr, ^{231}Pa/^{230}Th sedimentary ratios have always been equal to or greater than the production ratio (0.093), which means that this region not only buries the ^{231}Pa and ^{230}Th produced in the overlying water column but it also buries extra ^{231}Pa delivered from elsewhere in the ocean. Burial of extra ^{231}Pa is greatest during the Holocene, in which ^{231}Pa/^{230}Th values range from 0.172 (in 05PC) to 0.211 (in 35PC). Similarly, high ratios (0.209–0.227) during the last interglacial period (MIS5) are only achieved in two cores (38PC and 12TC/PC). In the other four cores, ^{231}Pa/^{230}Th values in MIS5 can only be classified as high when juxtaposed with the particularly low values in MIS6 (0.093–0.134). The near-production sedimentary ratios in MIS6 characterize the later glacial periods MIS2 and MIS4 as well, suggesting that the burial of extra ^{231}Pa on the Juan de Fuca Ridge is a phenomenon of warm interglacial intervals.

In addition to the glacial-interglacial variability in sedimentary ^{231}Pa/^{230}Th, four of the six cores (12TC/PC, 35PC, 38PC, and 39BB) capture a high ^{231}Pa/^{230}Th event (0.164–0.195) around 30 ka. Peculiarly, this feature does not appear in the core with the highest sedimentation rate in this interval (09PC, see Table 1), but its existence in the majority of the other cores as well as its constraint, at times, with more than one data point (e.g., 12TC/PC), suggests that it may be a real feature of the data. A peak in sedimentary ^{231}Pa/^{230}Th at 30 ka may conform with earlier peaks at 55, 71, 96, and 113 ka to create a quasi-precessional cycle. While the peak in 09PC at 96.5 ka approaches the interglacial values observed at ~125 ka (MIS5e) in 38PC and 12PC, this feature cannot be attributed to age model offsets. The age model is well constrained at glacial-interglacial transitions (Costa, McManus, Boulahanis, et al., 2016), and the oxygen isotopes and physical properties of 09PC firmly position the high ^{231}Pa/^{230}Th peak in late MIS5 (supporting information Figure S1). Thus, this peak at 96.5 ka in 09PC represents an additional ^{231}Pa burial event that is distinct from those older peaks at ~125 ka.

Because the glacial-interglacial trends captured in the six records are so similar, they can easily be combined into a single ^{231}Pa/^{230}Th stacked record (Figures 3a and 3b). The ^{231}Pa/^{230}Th stack averages all the data points within 2-kyr bins to generate a regional average record, and errors are calculated as the standard error of the

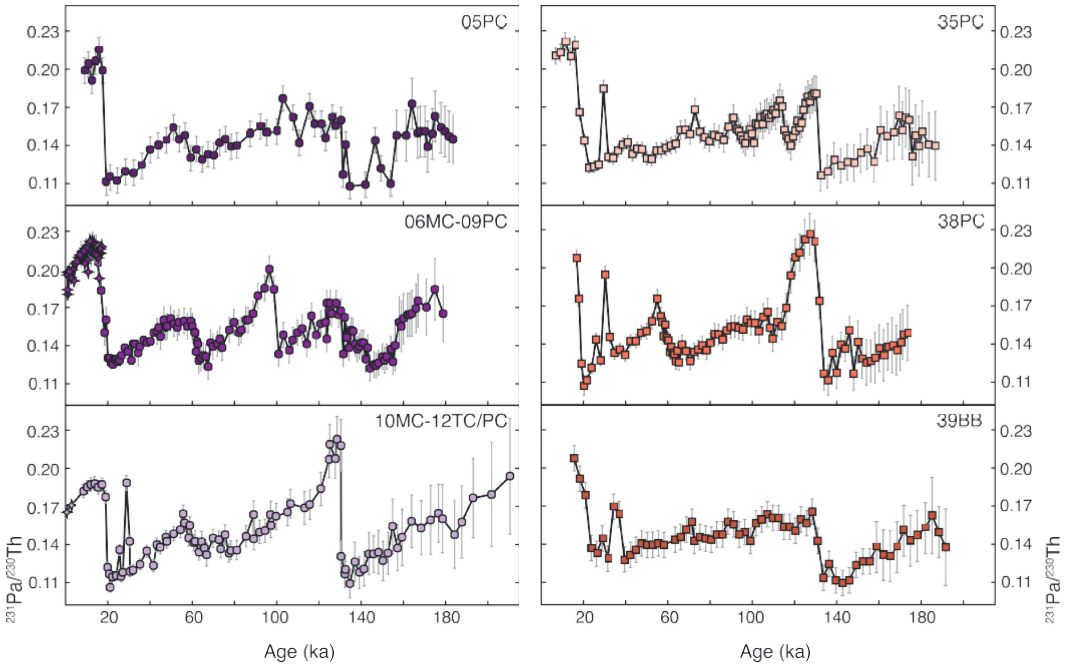

Figure 2. Individual $^{231}Pa/^{230}Th$ from the Juan de Fuca Ridge. All data points are greater than or equal to the production ratio in the overlying water column (0.093), indicating that this region is characterized by boundary scavenging. Error bars show 2σ. For 09PC and 12TC/PC, stars indicate data from multicores 06MC and 10MC, respectively. Sedimentary $^{231}Pa/^{230}Th$ ratios track climate, with high burial ratios during interglacial periods and low burial ratios during glacial periods. Peak in 09PC at ~100 ka is distinct from the later peak at ~125 ka observed in other cores and cannot be attributed to age model error (supporting information Figure S1).

data points within each bin. The stacked record (Figure 3b) is characterized by high interglacial values in MIS5 (0.183–0.190) and MIS1 (0.203–0.211) and low glacial values in MIS6 (0.123–0.136) and MIS2 (0.125–0.127).

Higher-frequency variability is retained with peaks in $^{231}Pa/^{230}Th$ at 29, 55, and 73 ka, and step changes from higher to lower $^{231}Pa/^{230}Th$ at 158 and 87 ka, but the peaks in $^{231}Pa/^{230}Th$ at 96 and 113 ka captured by individual cores are lost in the regional compilation. Overall, the major feature of the long JdFR $^{231}Pa/^{230}Th$ record is its remarkable consistency with climate (Figure 3), as seen in the regional benthic oxygen isotope stack from the JdFR (Costa, McManus, Boulahanis, et al., 2016).

4. Discussion

4.1. $^{231}Pa/^{230}Th$ as a Productivity Proxy in the Subarctic Pacific

Sedimentary $^{231}Pa/^{230}Th$ in the modern Pacific Ocean is largely driven by opal scavenging (Hayes et al., 2014), suggesting that $^{231}Pa/^{230}Th$ should be an effective indicator for changes in productivity in the past. Comparisons of $^{231}Pa/^{230}Th$ and other paleoproductivity proxies (e.g., opal fluxes) in the Pacific often yield highly positive correlations (Bradtmiller et al., 2006; Costa et al., 2016), but the relationship is stronger in some regions than in others (Dubois et al., 2010; Lam et al., 2013; Pichat et al., 2004). Some degree of interproxy disagreement is not uncommon when reconstructing productivity (e.g., see discussions in Anderson & Winckler, 2005; Kohfeld & Chase, 2011; Serno et al., 2014), and for $^{231}Pa/^{230}Th$ it arises because (1) $^{231}Pa/^{230}Th$ may be integrating different kinds of productivity (e.g., diatomaceous vs. coccolithophorid) and (2) organic components are susceptible to postdepositional changes in preservation and diagenesis.

Opal scavenges $^{231}Pa/^{230}Th$ due to both the particle-flux effect and the particle composition effect, and therefore, opal and $^{231}Pa/^{230}Th$ should be highly correlated in regions where surface productivity is domi- nated specifically by diatoms and other siliceous biota. Where nonsiliceous biota constitute an important component of the surface ecology, high productivity may increase scavenging due to the particle flux effect alone, thus elevating sedimentary $^{231}Pa/^{230}Th$ independent of opal. The disparate trends in organic carbon, excess barium, and opal fluxes from these sites on the JdFR (Costa et al., 2018) suggest that productivity in

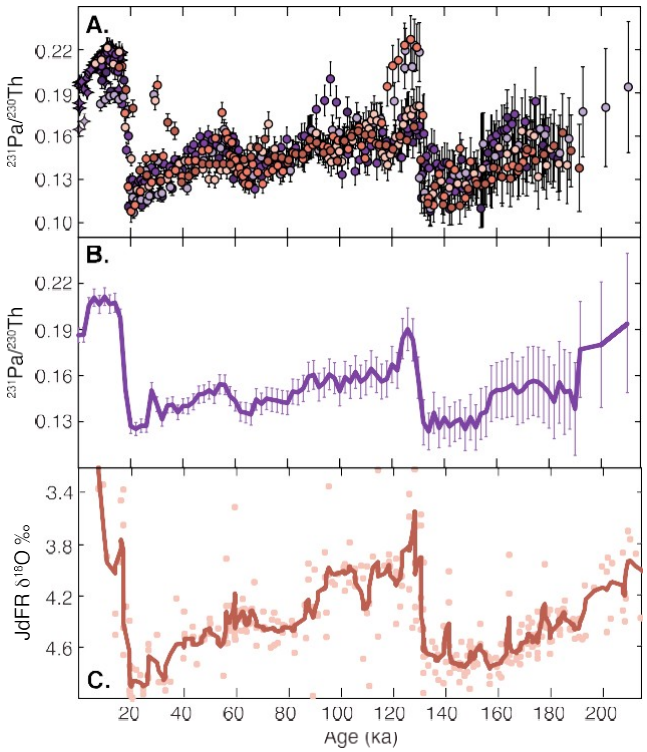

Figure 3. Compiled $^{231}Pa/^{230}Th$ records for the past 210 ka. (a) Individual datapoints from the Juan de Fuca Ridge overlain in the same panel, using the color scheme in Figure 2 to identify each of the study cores. Error bars show 2σ. (b) Stacked $^{231}Pa/^{230}Th$ record from the Juan de Fuca Ridge. Data points from all six sites were averaged in 2-kyr bins, and error bars represent 2 standard error. Burial ratios are always higher than the production rate (0.093). (c) Juan de Fuca Ridge benthic $\delta^{18}O$ record (Costa, McManus, Boulahanis, et al., 2016), to which stacked $^{231}Pa/^{230}Th$ record is quite similar.

this region may be diverse, and so the relationship between sedimentary $^{231}Pa/^{230}Th$ and productivity is likely to be nonlinear.

Preservation and diagenesis can have an even greater confounding effect on paleoproductivity reconstruction, because the specific environmental parameters controlling preservation are unique to each proxy (Anderson & Winckler, 2005; Kohfeld & Chase, 2011). For example, organic carbon is sensitive to oxygen concentrations in bottom and pore waters (e.g., Arndt et al., 2013; Ganeshram et al., 1999; Hedges et al., 1999), but its pre- servation is additionally affected by benthic activity and bioturbation (Canfield, 1994; Hartnett et al., 1998), host sediment composition (Keil et al., 1994; Keil & Hedges, 1993), and sedimentation rates (Müller & Suess, 1979). Excess barium, primarily in the form of barite (Dymond et al., 1992; Hernandez-Sanchez et al., 2011), is sensitive to sedimentary redox conditions (Dymond et al., 1992; Eagle et al., 2003; Hernandez- Sanchez et al., 2011; McManus et al., 1994, 1998; Paytan & Griffith, 2007; Torres et al., 1996; van Os et al., 1991), such that under substantial sulfate reduction, barite dissolves and releases barium back to the pore waters, reducing or even eliminating any productivity record in that sedimentary proxy (Dickens, 2001; Dymond et al., 1992; Schenau et al., 2001). Dissolution of opal is omnipresent on the seafloor, since seawater is always undersaturated in dissolved silica, and thermodynamically, opal will dis- solve until the pore water concentrations of silica reach equilibrium (Archer et al., 1993; Ragueneau et al., 2000). Kinetically, the rate of opal dis- solution will depend on the abundance of structural flaws (Van Cappellen & Qiu, 1997), organic and inorganic coatings (Ragueneau et al., 2000), water saturation (Archer et al., 1993; Ragueneau et al., 2000), trace metal defects (Archer et al., 1993; Nelson et al., 1995; Treguer & de la Rocha, 2013), and resilience of the diatom assemblage (Grigorov et al., 2014). The influence of preservation biases on opal flux at the JdFR is suggested by the nearly exponential decay in opal flux with age (Figure 4b), which would be consistent with increasing opal dissolution over time.

The extent of opal diagenesis may be quite extreme, as evidenced by a comparison of opal flux with Si_{xs} flux (Figure 4). In practice, opal is operationally defined by the silica that can be leached from the sediment in an alkaline solution (e.g., Mortlock & Froelich, 1989). Any biogenic silica that metamorphizes into an unleachable mineral phase, for example, through reaction with Al, Fe, and Mg in the surrounding sedimentary matrix (Archer et al., 1993; Cole, 1985; Dixit et al., 2001; Nelson et al., 1995; Treguer & de la Rocha, 2013), may not be recoverable as opal. In such a case, the reconstructed opal fluxes would underestimate the original opal signal at the time of burial (Rahman et al., 2016). The loss of opal by diagenetic transformation may be quantified by measuring Si_{xs} fluxes, which are insensitive to the mineralogy of the silica in the sediment. At the JdFR, opal and Si_{xs} fluxes indicate similar productivity trends for the last 50 kyr (Figure 4), but they diverge in the older part of the record, when Si_{xs} fluxes suggest much higher levels of productivity during the last interglacial period (MIS5) than opal. In fact, Si_{xs} fluxes suggest that opal productivity during MIS5 (13.4 mg/cm^2 kyr) was similar to that of the Holocene (15.2 mg/cm^2 kyr), in contrast to the nearly 65% lower productivity suggested by opal in MIS5 (10.0 mg/cm^2 kyr) versus the Holocene (28.3 mg/cm^{2}kyr). If this loss of opal could be attributed to transformation into nonopalline phases, it may indicate that the reverse weathering reaction (Mackenzie & Kump, 1995; Michalopoulos et al., 2000; Sillen, 1961) can occur at a relatively rapid rate if conditions are appropriate (Rahman et al., 2016). Future work on opal diagenesis might focus on the miner- alogy of the sedimentary matrix and the resulting nonopalline silica-rich phases in order to provide greater understanding of the environments that may reduce the utility of opal as a productivity proxy.

One of the main advantages of $^{231}Pa/^{230}Th$ over opal, as well as over other productivity proxies, is its relative insensitivity to changes in preservation and diagenesis (Chase et al., 2003; Pichat et al., 2004). The limited solubility of both ^{231}Pa and ^{230}Th increases the likelihood that even if their original host particle dissolved,

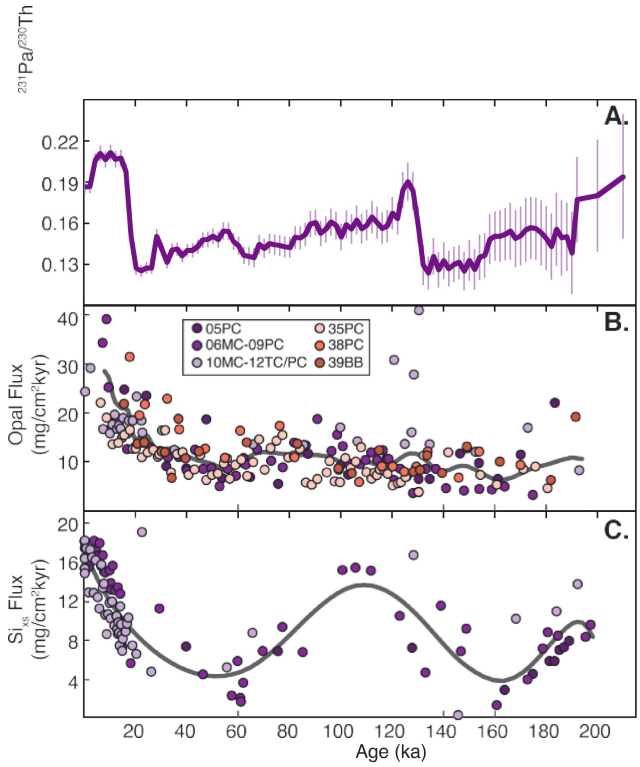

Figure 4. Preservation effects on opal. (a) $^{231}Pa/^{230}Th$ stack, as in Figure 3. (b) Opal fluxes, calculated with ^{230}Th-normalized fluxes (Costa et al., 2018). (c) Excess silica (Si_{xs}) fluxes, calculated with ^{230}Th-normalized fluxes. Gray lines show general trends based on 10-pt smoothing (b) and best polynomial fit (c). Legend in (b) also applies to (c). Both opal and Si_{xs} fluxes show increasing trends for the last 50 kyr, but they differ in the older part of the record (>50 ka). Si_{xs} fluxes show similar levels of productivity during MIS5 and the Holocene, while opal fluxes suggest productivity was two thirds lower in MIS5 compared to the Holocene.

these nuclides would most likely adsorb onto an adjacent particle in the sedimentary pile rather than diffuse through the pore water and out of the sediment as dissolved ions (Francois et al., 2004; Henderson & Anderson, 2003). Thus, $^{231}Pa/^{230}Th$ is likely to be the most robust and reli- able productivity indicator currently available.

4.2. Glacial-Interglacial Variability in Productivity in the Subarctic Pacific

Low productivity during cold periods is a pervasive feature of the Subarctic Pacific, on both million year (Haug et al., 2005; Sigman et al., 2004) and orbital timescales (Galbraith et al., 2007; Jaccard et al., 2005; Kienast et al., 2004; Okazaki et al., 2005; Okazaki et al., 2005). Long (>60 kyr) pro- ductivity records from across the region (Figure 5) show generally coher-
ent glacial-interglacial variability in the open ocean (West and East Subarctic) and in the marginal seas (Bering and Okhotsk Sea). In all but one core from the Okhotsk Sea, productivity peaks in MIS5 and the Holocene and reaches minima in MIS2 and MIS4. Regional differences are more apparent on subglacial timescales. In the West and East Subarctic, productivity varies with mean global climate, as represented by the LR04 benthic $\delta^{18}O$ stack (Lisiecki & Raymo, 2005), such that there is an early interglacial maximum (MIS5e), followed by relatively high inter- glacial productivity (MIS5a–MIS5d), a step decrease in productivity that coincides with glacial onset (MIS4), a return to higher productivity during the warm MIS3, a minimum at the last glacial maximum (MIS2), and a rapid increase in productivity during the last deglaciation. This subglacial varia- bility is somewhat evident in the Okhotsk Sea but notably absent in the Bering Sea, where productivity hovers at low background values except for the few peaks that occur in interglacial periods. Thus, high productivity occurs only but not always during warm climate periods in marginal seas, while it always responds to climate cycles in the open ocean.

The apparent climate dependency of productivity is primarily attributed to changes in stratification in the Subarctic Pacific, akin to those of the Antarctic Zone of the Southern Ocean (Basak et al., 2018; Francois et al., 1997; Mortlock et al., 1991; Robinson et al., 2004; Sigman et al., 2004). Stratification and density-driven mixing control nutrient delivery to the surface in the modern Subarctic Pacific, because high precipitation relative to evaporation (P-E) creates a low-salinity surface cap that is so fresh that even near-freezing winter temperatures are insufficient for densification and deep water formation (Emile-Geay et al., 2003; Warren, 1983). Average mixed layer depths in the East Subarctic are only 50 m in the summer, too shallow to reach nutrient-rich deep waters, but can extend up to 100 m in the winter, so that annual average nutrient concentrations in surface waters are almost entirely dependent on deep winter mixing (Glover et al., 1994; Tabata, 1975; Whitney, 2011; Whitney & Freeland, 1999). Seasonality is even stronger in the West Subarctic, where mixing reaches less than 50 m in the summer but 150 m or more in the winter (Glover et al., 1994; Honda et al., 2002), leading to higher nutrient concentrations in surface waters of the west (Harrison et al., 1999). Across the Subarctic region, the main growing season (May–September) begins (Harrison et al., 1999) in the spring when the nutrient-rich winter mixed layer stratifies and light limitation is relieved. Without continued replen- ishment the nutrient supply progressively declines through the summer (Kawakami et al., 2007; Whitney, 2011; Whitney & Freeland, 1999; Wong et al., 2002) until further production is limited by iron availability (Boyd & Harrison, 1999; Martin & Fitzwater, 1988; Tsuda et al., 2005). Integrated over tens to hundreds of years, the average nutrient concentrations in surface waters are set by the rates of winter mixing versus sum- mer drawdown, that is, net nutrient utilization.

High dust fluxes during glacial periods (e.g., McGee et al., 2010; Serno et al., 2015; Serno et al., 2017; Winckler et al., 2008) would have likely increased surface iron concentrations, a boon to iron-limited waters that would have promoted high productivity, rather than the low productivity that is actually observed. The combination of low glacial productivity (Figure 5), high iron availability, and high nutrient utilization (Ren et al., 2015)

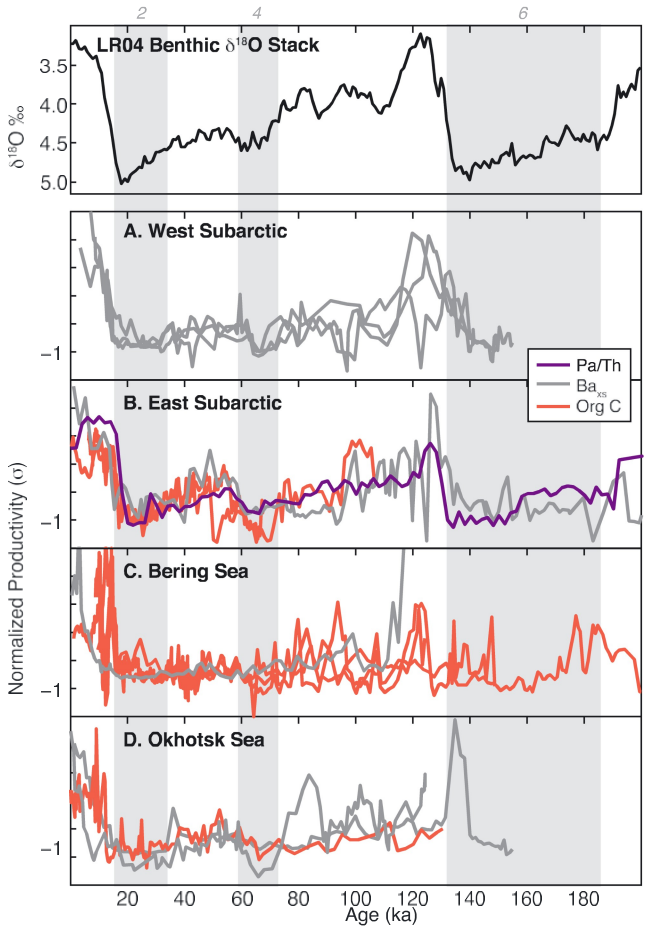

Figure 5. Other long productivity records from the Subarctic Pacific. Records are color coded based on the proxy used and grouped based on region. Organic carbon (Org C) and excess barium (Ba_{xs}) were corrected for changes in dilution based on calcium carbonate content and opal content, since ^{230}Th-based flux calculations were not feasible. All records have been normalized (*z* scored) by subtracting the mean and dividing by the standard deviation in order to facilitate plotting on the same scale. (a) West Subarctic: ODP882 (Jaccard et al., 2009), RNDP-PC13 (Brunelle et al., 2010), and MR98- 05-3PC (Shigemitsu et al., 2007). (b) East Subarctic: JdFR (this study), W8709-8 and W8709-13 (Kienast, 2003), and ODP887 (McDonald et al., 1999).
(c) Bering Sea: SO201-2-85 and SO201-2-77 (Riethdorf, Nurnberg, et al., 2013), U1342 (Knudson & Ravelo, 2015a), and JPC17 (Brunelle et al., 2007).
(d) Okhotsk Sea: PC936 (Gorbarenko et al., 2004), GGC27 (Brunelle et al., 2010), and X98-01PC (Sato et al., 2002). Top panel shows the LR04 benthic δ^{18}O stack for climatic context (Lisiecki & Raymo, 2005). Gray bars highlight glacial periods, identified by even Marine Isotope Stages (gray numbers at top).

indicates reduced nutrient supply to the euphotic zone during glacial periods (Jaccard et al., 2010), which may have evolved as result of several possible mechanisms. A fresher surface layer, saltier deep layer, or both would create a stronger pycnocline that would impede mixing to significant depths (Zahn et al., 1991), while a thicker volume of low-density surface water would depress nutrient-rich deep waters out of reach of the mixed layer depth. A decrease in wind strength would shoal mixing depths, potentially enhancing the stratifying effects of coincident changes to the pycnocline. Also, a reduction of nutrient concentrations in the subsurface water would limit the resupply of nutrients to the surface during mixing, in addition to any changes to the physical mixing regime. These processes are not mutually exclusive, and all would contribute to the umbrella mechanism of increased glacial stratification. In the next sections, we con- sider the current evidence for or against each of these mechanistic compo- nents for reducing nutrient delivery to the glacial surface ocean.

4.2.1. Strengthening the Pycnocline

The primary element that contributes to physical stratification is the vertical density profile of the upper ocean (0–200 m). The depth and intensity (strength of the gradient) of the pycnocline acts as a resistor against the downward mixing forces applied at the surface (such as wind strength; see next section). A steep pycnocline (large change in density over a short depth interval) creates a diapycnal barrier against which the available energy for mixing is rapidly consumed, and a near-surface pycnocline places this barrier high in the water column, further limiting the mixed layer depth. The polar stratification hypothesis suggests that simply cool- ing the entire water column (as during a glacial period) can be sufficient to strengthen the pycnocline due to the non-linear temperature depen- dence of the equation of state (Sigman et al., 2004). In the Antarctic Ocean, the steepness of the pycnocline doubles when the entire water col- umn is cooled by 2°C (Sigman et al., 2004). Conversely, in the Subarctic Pacific, cooling has the opposite effect on density profiles (Figure 6), based on reproducing the Sigman et al. (2004) calculations on a representative temperature and salinity profile from Station PAPA. Cooling the water col- umn by 2°C actually weakens the density gradient in the upper ocean (σ_{200m}–σ_{0m}) from 1.047 g/m^3 (today) to 1.017 kg/m^3 (simulated glacial per- iod). Continuing to cool the water column all the way to the freezing point (−1.9°C) only further weakens the density gradient, to 0.8958 kg/m^3. Only by also decreasing the surface salinity (by 0.5 in the upper 100 m, in this example) relative to the rest of the water column does the pycnocline stee- pen, with an increased density gradient of 1.39 kg/m^3. The dissimilar response of Subarctic Pacific and Antarctic density profiles is likely driven by the order of magnitude steeper halocline in the Subarctic Pacific (change in salinity of 1.1) compared to the Antarctic (change in salinity of 0.2, in Sigman et al., 2004), giving salinity much more influence over the density profiles in the Subarctic Pacific than in the Antarctic. A consequence of the dominance of salinity in the Subarctic Pacific is that glacial cooling cannot, on its own, generate enhanced stratification, as it can in the Antarctic. Additional processes reducing the salinity of surface waters during glacial periods must also be invoked in order to create the steep density profiles that characterize stratification.

One mechanism for freshening surface waters may have been the glacial closure of the Bering Strait, which reduced freshwater export out of the Pacific. In the modern ocean, approximately 1 Sv of relatively fresh water flows through the shallow (50 m) strait from the Pacific to the Atlantic via the Arctic (Talley, 2008). Lower sea level during the glacial period would have cut off this pathway and retained that freshwater flux in the North Pacific (Keigwin & Cook, 2007), and the opening and closure of the Bering Strait may be a

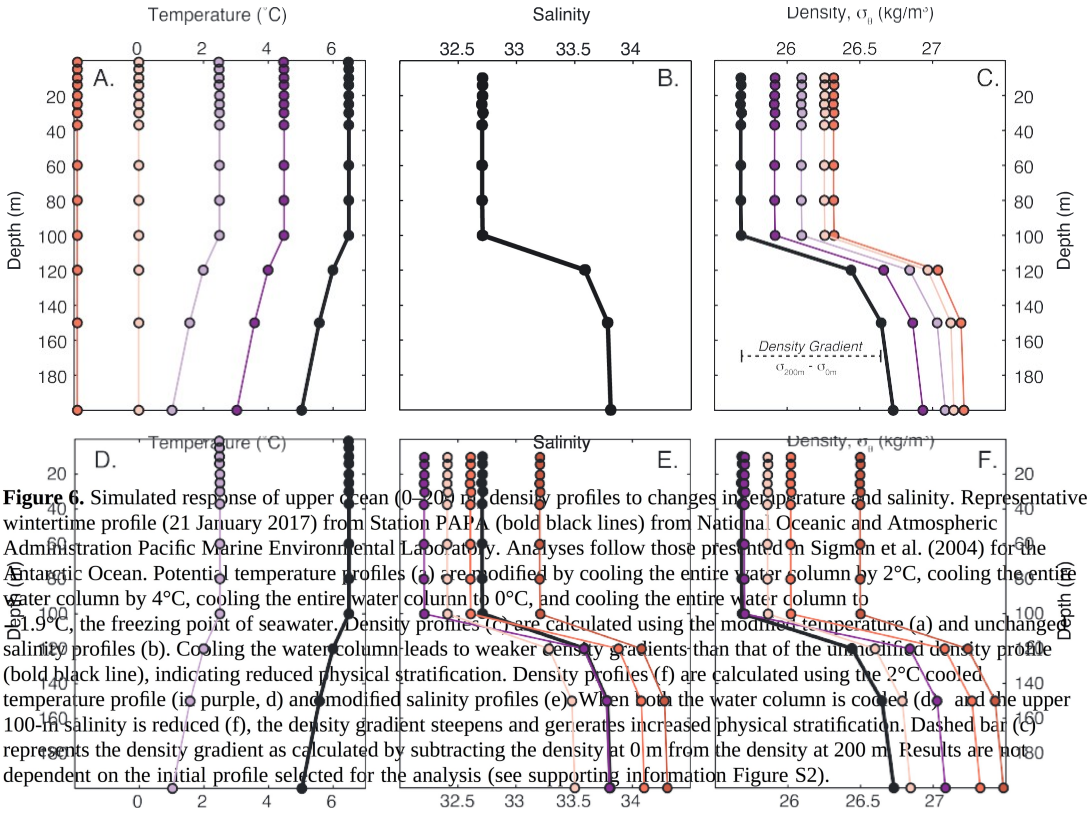

Figure 6. Simulated response of upper ocean (0–200 m) density profiles to changes in temperature and salinity. Representative wintertime profile (21 January 2017) from Station PAPA (bold black lines) from National Oceanic and Atmospheric Administration Pacific Marine Environmental Laboratory. Analyses follow those presented in Sigman et al. (2004) for the Antarctic Ocean. Potential temperature profiles (a) are modified by cooling the entire water column by 2°C, cooling the entire water column by 4°C, cooling the entire water column to 0°C, and cooling the entire water column to −1.9°C, the freezing point of seawater. Density profiles (c) are calculated using the modified temperature (a) and unchanged salinity profiles (b). Cooling the water column leads to weaker density gradients than that of the unmodified density profile (bold black line), indicating reduced physical stratification. Density profiles (f) are calculated using the 2°C cooled temperature profile (a, purple, d) and modified salinity profiles (e). When both the water column is cooled (d) and the upper 100-m salinity is reduced (f), the density gradient steepens and generates increased physical stratification. Dashed bar (c) represents the density gradient as calculated by subtracting the density at 0 m from the density at 200 m. Results are not dependent on the initial profile selected for the analysis (see supporting information Figure S2).

toggle between Atlantic Meridional Overturning Circulation (MOC) and Pacific MOC on glacial-interglacial timescales (De Boer & Nof, 2004; Hu et al., 2010, 2015; Hu, Meehl, Han, Abe-Ouchi, et al., 2012; Hu, Meehl, Han, Timmermann, et al., 2012; Shaffer & Bendtsen, 1994). Only one study has modeled the consequent influence of Bering strait closure on sea surface salinity in the Subarctic Pacific, generating a spatially heterogeneous decrease in sea surface salinity of up to 1 (Hu et al., 2010). The relatively coherent productivity records (Figure 5) are inconsistent with simulated regionally specific changes in surface salinity and stratification, but it is unclear if these patterns would be robust with integration over longer time periods. Future efforts on modeling the spatial patterns of sea surface salinity during glacial periods will help corroborate the distribution of freshwater and the potential role for closure of the Bering Strait on stratification in the glacial Subarctic Pacific.

An additional mechanism to redistribute salinity, add freshwater to the surface, and generate physical stratification in the Subarctic Pacific may be the formation, transport, and melting of sea ice (Gorbarenko, 1996; Keigwin et al., 1992; Sancetta, 1983; Seki et al., 2004). Sea ice forms in the wintertime in the Okhotsk and Bering Seas, and localized brine rejection in thin coastal margin regions removes buoyancy from near-surface waters enough to create North Pacific Intermediate Water (NPIW) (Shcherbina et al., 2003). Because winds

blow the sea ice away from their originating polynyas (Pease, 1980; Sakamoto et al., 2005), brine rejection occurs repeatedly in the same spatially limited location, in a densification process that is distinct and independent from deep vertical mixing (and nutrient supply). Sequestering the relatively saline water into the NPIW at subsurface depths (>50 m) allows for a net freshening of surface waters (0–50 m) (Hillaire-Marcel & de Vernal, 2008), which retain the sea ice and meltwater. Enhanced formation and export of NPIW due to an amplified sea ice cycle during glacial periods (Artemova et al., 2017; Caissie et al., 2010; Katsuki & Takahashi, 2005; Sakamoto et al., 2005) may sufficiently freshen surface waters to instigate physical stratification and thus diminish productivity. Indeed, reconstructions of $\delta^{13}C$ from benthic foraminifera have identified a high $\delta^{13}C$, high εNd water mass above 2,000 m during the last glacial maximum that is attributed to a more vigorous NPIW (Cook et al., 2016; Horikawa et al., 2010; Jang et al., 2017; Keigwin, 1987, 1998; Knudson & Ravelo, 2015b; Matsumoto et al., 2002; Max et al., 2017).

Connecting NPIW formation with the sea ice cycle rather than focusing on a seesaw with Atlantic MOC (e.g., Freeman et al., 2015; Hu, Meehl, Han, Abe-Ouchi, et al., 2012; Menviel et al., 2017; Mikolajewicz et al., 1997; Okazaki et al., 2010) allows for enhanced NPIW formation even when Atlantic MOC is relatively strong (Böhm et al., 2015; Henry et al., 2016; Jonkers et al., 2015; Lynch-Stieglitz et al., 2007) and releases NPIW formation from the transience of millennial scale events that characterize Atlantic MOC variability (Boyle & Keigwin, 1987; Henry et al., 2016; McManus et al., 2004; Ng et al., 2018; Praetorius et al., 2008). Because sea ice expands as temperature cools, NPIW formation would follow global climate (e.g., Lisiecki & Raymo, 2005) and generate the glacial-interglacial cycles in physical stratification inferred from the productivity records. Furthermore, in contrast to previous studies that have anticipated spatial variabil- ity from sea ice effects (Brunelle et al., 2007, 2010), rapid advection across the Subarctic Pacific (1–2 years; Smith et al., 2015) would distribute freshwater fluxes on timescales consistent with the spatially homoge- neous productivity records. Thus, the sea ice-NPIW mechanism for generating physical stratification can account for both the spatially homogeneous productivity response as well as the link between stratifica- tion and global climate.

The sea ice-NPIW hypothesis could be tested by reconstructing the seawater $\delta^{18}O$ ($\delta^{18}O_{sw}$) profile of the upper ocean (0–200 m) over time. When sea ice forms, it fractionates $\delta^{18}O$ such that the ice is isotopically enriched and the residual brine is isotopically depleted (O'Neil, 1968), making sea ice formation the only pro- cess by which a negative correlation between $\delta^{18}O$ and salinity develops (Hillaire-Marcel & de Vernal, 2008). Thus, sea ice melt can be identified in surface waters (<50 m) by the presence of cold (fresh) and high $\delta^{18}O_{sw}$ water overlying saltier but lower $\delta^{18}O_{sw}$ water (subducted brines; Brennan et al., 2013; Hillaire-Marcel & de Vernal, 2008; Riethdorf et al., 2013). Such a profile may be constructed by analyzing paired $\delta^{18}O$ and temperature (e.g., Mg/Ca) in planktonic foraminifera that inhabit different depths in the surface ocean (Figure 7; e.g., Kumar et al., 2018; Parker et al., 2015; Wara et al., 2005). Although foraminiferal depth habitats appear to be highly variable across the Subarctic Pacific (Iwasaki et al., 2017; Kuroyanagi et al., 2008; Taylor et al., 2018), at any one station a depth distribution in foraminifera species is often observed. For example, plankton tows from Station PAPA suggest that *G. bulloides*, *G. quinqueloba*, and *N. incompta* are most abundant in the upper 50 m, while *N. pachyderma* and *O. universa* are most abundant in the 200- to 300-m depth (Iwasaki et al., 2017). Under normal conditions the surface (<50 m) to deep (200–300 m) $\delta^{18}O_{sw}$ gradient ($\Delta\delta^{18}O_{sw}{}^{200\text{-}0m}$) would be slightly positive (Figure 7a), according to the standard positive relationship between $\delta^{18}O_{sw}$ and density. During either winter sea ice formation (Figure 7b) or spring sea ice melt (Figure 7c), the $\delta^{18}O_{sw}$ gradient would invert, with higher $\delta^{18}O_{sw}$ observed in the surface (<50 m) species and a negative gradient with depth. This approach would, of course, have to contend with complicating factors such as the sensitivity of upper ocean $\delta^{18}O$ to perturbations in the sea ice, the seasonality of each planktonic species (e.g., Fraile et al., 2009; Reynolds & Thunell, 1985), the local depth habitats of different planktonic species (e.g., Iwasaki et al., 2017; Taylor et al., 2018), secondary influences on both $\delta^{18}O$ and Mg/Ca (e.g., Hönisch et al., 2013), and calibration uncertainties on Mg/Ca for each planktonic species (e.g., Anand et al., 2003). Yet unlike other sea ice proxies like diatom assemblages or IP_{25}, the $\Delta\delta^{18}O_{sw}{}^{200\text{-}0m}$ has the advantage of recording the distal extent of sea ice melt far from the sea ice margin as well as the in situ consequences of sea ice melt on stra- tification of the upper ocean (0–200 m). Future work to develop this proxy may contribute toward under- standing the density structure of the upper ocean and its effects on physical stratification, nutrient delivery to the surface, and thus productivity under glacial-interglacial climate conditions.

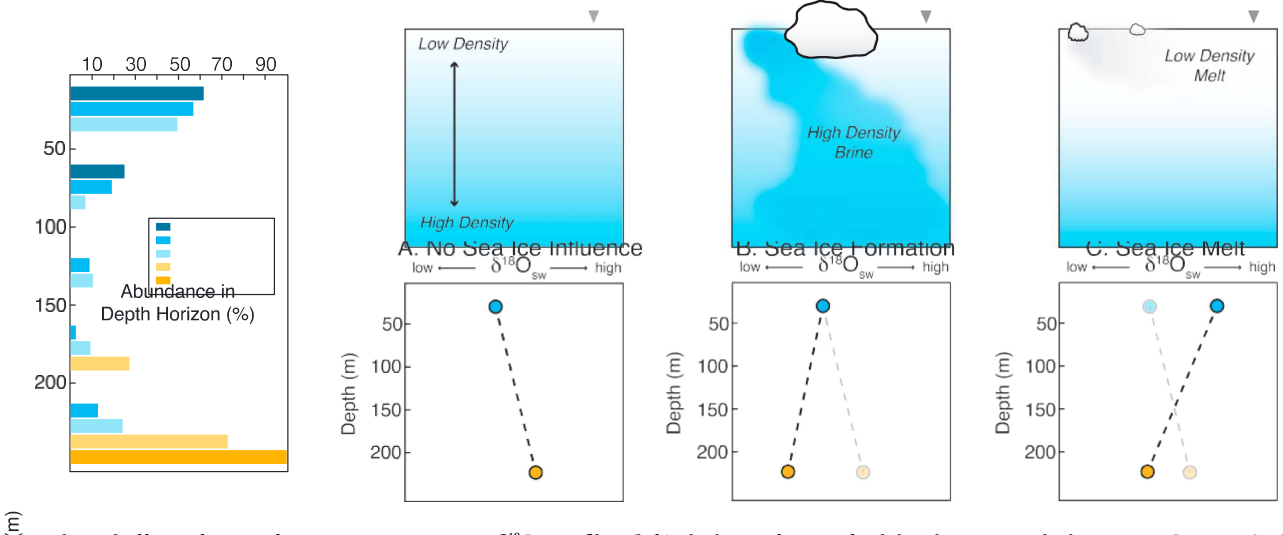

Figure 7. Hypothetical effects of sea ice formation on upper ocean $\delta^{18}O_{sw}$ profiles. (left) Planktonic foraminiferal distribution in a plankton tow at Station PAPA (Iwasaki et al., 2017). At least 50% of all *G. bulloides*, *G. quinqueloba*, and *N. incompta* were recovered within the 0- to 50-m depth, making these species the best candidates for recording shallow conditions. More than 70% of all *N. pachyderma* and *O. universa* were recovered from the 200- to 300-m depth, making these species the best candidates for recording subsurface conditions. (right) Hypothetical changes to upper ocean $\delta^{18}O_{sw}$ profiles recorded by shallow (blue) and subsurface (orange) foraminiferal species in response to different sea ice events. Gray triangles indicate the relative location for the water column profiles shown in the bottom panels. (a) When no sea ice is present, the $\delta^{18}O_{sw}$ gradient is positive. (b) During sea ice formation, high density, low $\delta^{18}O_{sw}$ brines invert the $\delta^{18}O_{sw}$ gradient. Faint line and circle show the initial profile as in scenario (a). (c) During sea ice melt, low density, high $\delta^{18}O_{sw}$ meltwater further enhances the negative $\delta^{18}O_{sw}$ gradient. Faint line and circles show the starting profile from (a).

4.2.2. Weaker Winds

Changes in wind strength may compound changes in the pycnocline to influence physical stratification (Figure 8). Wind forcing at the sea surface provides the energy to propel downward mixing. The depth of the mixed layer is thus a function of both the energy (wind strength) applied to and the resistance (density structure) within the surface ocean. For example, weak winds combined with a strong pycnocline would severely depress the winter mixing depth and nutrient delivery to the surface (e.g., Beaufort et al., 1997). On the other hand, if strong winds countered a strong pycnocline, the increased mixing energy might over- come the increased resistance to mixing, such that there may be no net change in the winter mixing depth. The influence of winds on mixing depth and nutrient delivery to the surface was directly observed during the strong El Niño of 1997–1998, when weakening of winds during winter 1997 (Sasaoka et al., 2002) resulted in lower than average surface nutrient concentrations the subsequent summer at station KNOT in the West Subarctic (Honda et al., 2002). In general, a positive correlation between the strength of winter winds and pri- mary productivity in the following summer has been observed in the Subarctic gyre in the twentieth century (Brodeur & Ware, 1992). Thus, considering how wind strength may have varied under glacial climate condi- tions is imperative to understanding the mechanisms behind enhanced physical stratification and surface nutrient delivery.

Globally, steeper meridional temperature gradients during the last glacial period predict stronger winds (McGee et al., 2010), particularly in the midlatitudes (Rind, 1998). Strong midlatitude jets are associated with an increase in eddy kinetic energy (storminess) (Penny et al., 2013), which should increase mixing depths and nutrient delivery to surface waters (O'Gorman, 2010). However, the presence of the Laurentide Ice Sheet likely deflected (or possibly bifurcated) the westerly storm track (Bromwich et al., 2004; COHMAP, 1988; Kirby et al., 2013; Oba et al., 2006; Oster et al., 2015), shifting it as much as 10° latitude to the south in the middle of the North Pacific (Lora et al., 2017; Figure 1). The more southerly storm track likely pushed this zone of storminess into the subtropical gyre, and models corroborate a net decrease in eddy kinetic energy over much of the Subarctic Pacific (Li & Battisti, 2008; Lora et al., 2017). This finding is consistent with modeled reductions of storminess over similar latitudes in the North Atlantic during the last glacial period (Dohonoe & Battisti, 2009; Li & Battisti, 2008; Riviere et al., 2018). Therefore, it seems likely that winds were weaker in the Subarctic Pacific during glacial compared to interglacial periods, and these weak winds potentially

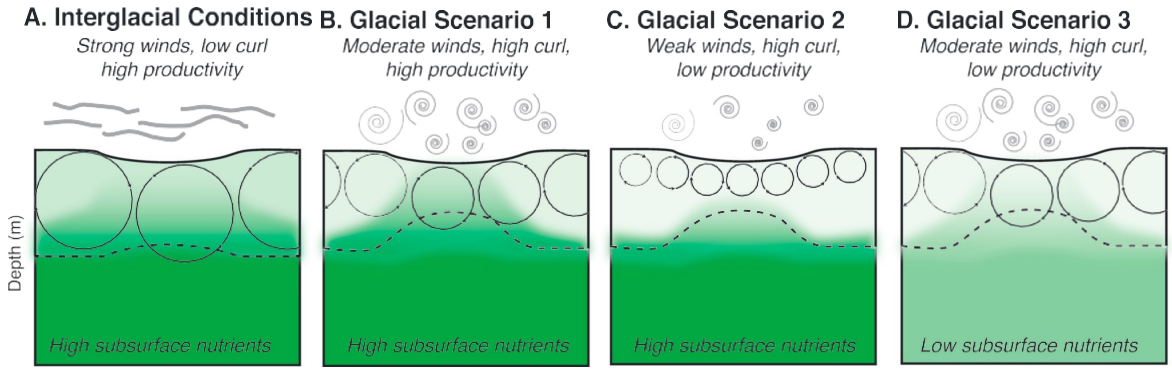

Figure 8. Hypothetical effects of changing winds on nutrient concentrations in the upper ocean. Schematic shows wind strength (gray lines), wind curl (spirality of gray lines), surface mixing (arrowed circles), nutricline (dashed line), and nutrient concentrations (green shading). (a) During interglacial periods, strong winds create deep mixing that can penetrate the high subsurface nutrients, despite a deep nutricline. Relatively high surface nutrient concentrations leads to high pro- ductivity. (b) During glacial periods, enhanced wind stress curl shoals the nutricline and moderate winds reduce the mixing depths. If the mixing depth intersects the nutricline, then surface nutrient concentrations would still remain high. This scenario is inconsistent with low glacial productivity in the Subarctic Pacific (Figure 5).
(c) Weak winds (or strong pycnocline, not shown) may reduce mixing depths so that they are unable to reach the nutrient rich subsurface waters. Nutrient con- centrations in the surface ocean remain low, consistent with low glacial productivity. (d) Surface mixing and nutricline as in (b), but with low subsurface nutrient concentrations. Upward mixing only supplies low nutrient concentrations to surface waters, consistent with low glacial productivity. A fourth glacial scenario could combine the weak winds of (c) and the low subsurface nutrients of (d) to also generate low glacial productivity.

contributed to reduced mixing depths, increased stratification, decreased nutrient delivery, and reduced productivity under glacial conditions.

In addition to powering winter mixing of surface waters, wind strength, and wind stress curl can also affect nutrient delivery to the surface by upwelling and Ekman divergence. Seasonal upwelling along the continen- tal margin delivers nutrient-rich subsurface waters (~100 m) to the surface (Wheeler et al., 2003), extending about 100 km off the coast (Whitney et al., 2005). These nutrients can be transported laterally by tidal mixing, eddy diffusion, and local turbulence (Whitney et al., 2005), so that coastal upwelling may be able to influence surface nutrient concentrations into the open ocean. Weak winds during glacial periods likely reduced coastal upwelling and repressed the potential nutrient leak from the coast to the open ocean. As all of the sites investigated here show similar patterns in productivity (Figure 5) regardless of distance from the coast, they do not appear to be sensitive to changes in the rates of coastal upwelling and nutrient leakage. Instead, they are more likely to respond to changes in the major source of nutrients in the subarctic gyre, Ekman diver- gence (Gargett, 1991; Reid, 1962).

Ekman divergence occurs within the subpolar gyre as a result of positive wind stress curl (Reid, 1962), and the rates of associated upwelling are more or less equivalent in the East and the West Subarctic (Gargett, 1991; Harrison et al., 1999). This upwelling leads to shoaling of the nutricline that may be sufficient to allow deep winter mixing to tap into those nutrient rich waters (Brodeur & Ware, 1992; Reid, 1962). During glacial periods, the wind stress curl would have increased in the Subarctic as the westerlies, the zero point of wind stress curl (Thomson, 1981), shifted southward and away from the Subarctic (Figure 8). Indeed, models suggest that wind stress curl may have been as much as 60% higher in this region during the last glacial period (Gray et al., 2018), increasing Ekman divergence and shoaling sub-surface waters. Yet glacial productivity was still lower than interglacial productivity. This contradiction between high rates of upwelling and low productivity can be reconciled either by particularly weak surface mixing or by low subsurface nutrient concentrations. If the decrease in mixing depth outpaced the shoaling of the nutricline, it is possible that the mixing depths were insufficient to breach the nutrient rich subsurface waters (Figure 8c), due to either very weak winds or a strong pycnocline (section 4.2.1). Alternatively, surface mixing may have intersected the subsurface waters, but nutrient concentrations of those waters may have been lower during glacial periods than during interglacial periods (Figure 8d). In either case, changes to wind stress do not appear to have been the primary driving force for changes in productivity on glacial-interglacial timescales.

4.2.3. Reduced Subsurface Nutrient Concentrations

Changes in ocean ventilation suggest that reduced subsurface nutrient concentrations may have been char- acteristic of the glacial Subarctic (Jaccard et al., 2010; Lam et al., 2013). This mechanism is based on the

chemical properties of water masses, and it is distinct from physical stratification, although the two are sometimes considered homologous. Today, deep winter mixing reaches depths of ~150 m and intersects with high subsurface nutrient concentrations (Figure 8a), propagating those high nutrients into surface waters. Nutrient concentrations within subsurface waters (>150 m) are a balance between mixing of young, nutrient-poor NPIW formed in the Okhotsk Sea (Talley, 1993; You, 2003) and old, nutrient-rich North Pacific Deep Water,

and modern NPIW is characterized by a steep vertical seawater $\delta^{13}C$ gradient from high $\delta^{13}C$ at the surface to low $\delta^{13}C$ at depth (Kroopnick, 1985). Enhanced NPIW formation during glacial periods (see section 4.2.1) expanded the high $\delta^{13}C$ (low nutrient) water mass to 2,000 m (Keigwin, 1998; Matsumoto et al., 2002), pushing the nutrient-rich North Pacific Deep Water to greater depths (Boyle, 1988), and reducing the nutrient concentrations of subsurface waters potentially attainable by winter mixing (Gray et al., 2018). Thus, lower subsurface nutrient concentrations likely combined with weaker winds and enhanced surface freshening to reduce productivity during glacial periods.

5. Conclusions

Productivity across the Subarctic Pacific varies coherently with glacial-interglacial cycles, with low productivity characterizing glacial periods in the open ocean and the marginal seas in both the east and the west. Stratification of surface waters has been suggested as the main driver of variability in productivity, and here we investigated the potential mechanisms for generating both physical and chemical stratification during glacial periods. Cooling of the water column alone is insufficient to increase the density gradient of the upper ocean (0–200 m), but increased freshwater inputs to the surface may have contributed to a steeper pycno- cline. Possible freshwater sources include sea ice melt and closure of the Bering Strait. Weaker winds, due to a southward shift of the westerlies, may have reduced the surface mixing depths, limiting nutrient supply to the surface, but increased wind stress curl would have increased upwelling and shoaled the nutricline, making subsurface waters more accessible to even shallow mixing. A near-surface nutricline may be reconcil- able with low glacial productivity if the subsurface nutrient concentrations were also low, perhaps due to enhanced NPIW formation or flushing or subsurface waters during glacial periods. In summary, low glacial productivity was caused by physical stratification and low surface nutrient concentrations induced by reduced surface mixing (weak winds and strong pycnocline) combined with upwelling of nutrient-poor subsurface waters.

Acknowledgments

The authors thank Martin Fleisher for technical assistance with U-Th-Pa chemistry and ICP-MS analysis at LDEO, and Frank Pavia for helpful discussion, brainstorming, and reality checks. The authors also appreciate valuable feedback from two anonymous reviewers that helped to improve this manuscript. Data are publically available in the Paleoclimate Data Repository of the NOAA National Climatic Data Center at https://www.ncdc.noaa.gov/paleo- search/study/24190. This research was funded in part by NSF award AGS- 1502889 to J. F. M. and a NSF Graduate Research Fellowship to K. M. C.

References

Addison, J. A., Finney, B. P., Dean, W. E., Davies, M. H., Mix, A. C., Stoner, J. S., & Jaeger, J. M. (2012). Productivity and sedimentary d15N variability for the last 17,000 years along the northern Gulf of Alaska continental slope. *Paleoceanography*, *27*, PA1206. https://doi.org/10.1029/2011PA002161

Anand, P., Elderfield, H., & Conte, M. H. (2003). Calibration of Mg/Ca thermometry in planktonic foraminifera from a sediment trap time series. *Paleoceanography*, *18*(2), 1050. https://doi.org/10.1029/2002PA000846

Anderson, R. F., Bacon, M. P., & Brewer, P. G. (1983). Removal of ^{230}Th and ^{231}Pa at ocean margins. *Earth and Planetary Science Letters*, *66*, 73–90.

Anderson, R. F., Lao, Y., Broecker, W. S., Trumbore, S. E., Hofmann, H. J., & Wolfli, W. (1990). Boundary scavenging in the Pacific Ocean: A comparison of ^{10}Be and ^{231}Pa. *Earth and Planetary Science Letters*, *96*, 287–304.

Anderson, R. F., & Winckler, G. (2005). Problems with paleoproductivity proxies. *Paleoceanography*, *20*, PA3012. https://doi.org/10.1029/2004PA001107

Archer, D., Lyle, M., Rodgers, K., & Froelich, P. (1993). What controls opal preservation in tropical deep-sea sediments. *Paleoceanography*, *8*(1), 7–21. https://doi.org/10.1029/92PA02803

Arndt, S., Jørgensen, B. B., LaRowe, D. E., Middelburg, J. J., Pancost, R. D., & Regnier, P. (2013). Quantifying the degradation of organic matter in marine sediments: A review and synthesis. *Earth-Science Reviews*, *123*, 53–86. https://doi.org/10.1016/j.earscirev.2013.02.008

Artemova, A., Gorbarenko, S., Vasilenko, Y., Shi, X., Liu, Y., & Chen, M. (2017). Palaeoceanography changes in the Okhotsk Sea during Late Pleistocene and Holocene according to diatoms. *Quaternary International*, *459*, 175–186. https://doi.org/10.1016/j.quaint.2017.10.002

Bacon, M. P. (1988). Tracers of chemical scavenging in the ocean: Boundary effects and large-scale chemical fractionation. *Philosophical Transactions. Royal Society of London*, *325*, 147–160.

Basak, C., Fröllje, H., Lamy, F., Gersonde, R., Benz, V., Anderson, R. F., et al. (2018). Breakup of last glacial deep stratification in the South Pacific. *Science (80-.)*, *904*(February), 900–904. https://doi.org/10.1126/science.aao2473

Beaufort, L., Lancelot, Y., Camberlin, P., Cayre, O., Vincent, E., Bassinot, F., & Labeyrie, L. (1997). Insolation cycles as a major control of equa- torial Indian Ocean primary production. *Science*, *278*(November), 1451–1454.

Böhm, E., Lippold, J., Gutjahr, M., Frank, M., Blaser, P., Antz, B., et al. (2015). Strong and deep Atlantic meridional overturning circulation during the last glacial cycle. *Nature*, *517*, 73–76. https://doi.org/10.1038/nature14059

Bonatti, E., Fisher, D. E., Joensuu, O., & Rydell, H. S. (1971). Postdepositional mobility of some transition elements, phosphorus, uranium and thorium in deep sea sediments. *Geochimica et Cosmochimica Acta*, *35*(2), 189–201. https://doi.org/10.1016/0016-7037(71)90057-3

Bostrom, K., & Peterson, M. N. A. (1966). Precipitates from hydrothermal exhalations on the East Pacific Rise. *Economic Geology*, *61*, 1258–1265.

Boyd, P. W., & Harrison, P. J. (1999). Phytoplankton dynamics in the NE subarctic Pacific. *Deep Sea Research, Part II*, *46*(11–12), 2405–2432.
Boyle, E. A. (1988). Vertical oceanic nutrient fractionation and glacial/interglacial CO_2 cycles. *Nature*, *331*(6151), 55–56. https://doi.org/10.1038/331055a0
Boyle, E. A., & Keigwin, L. D. (1987). North Atlantic thermohaline circulation during the past 20,000 years linked to high latitude surface temperature. *Nature*, *350*, 35–40.
Bradtmiller, L. I., Anderson, R. F., Fleisher, M. Q., & Burckle, L. H. (2006). Diatom productivity in the equatorial Pacific Ocean from the last glacial period to the present: A test of the silicic acid leakage hypothesis. *Paleoceanography*, *21*, PA4201. https://doi.org/10.1029/2006PA001282 Brennan, C. E., Meissner, K. J., Eby, M., Hillaire-Marcel, C., & Weaver, A. J. (2013). Impact of sea ice variability on the oxygen isotope content of seawater under glacial and interglacial conditions. *Paleoceanography*, *28*, 388–400. https://doi.org/10.1002/palo.20036 Brodeur, R. D., & Ware, D. M. (1992). Long-term variability in zooplankton biomass in the subarctic Pacific Ocean. *Fisheries Oceanography*, *I*(I), 32–38. https://doi.org/10.1111/j.1365-2419.1992.tb00023.x
Bromwich, D. H., Toracinta, E. R., Wej, H., Oglesby, R. J., Fastook, J. L., & Hughes, T. J. (2004). Polar MM5 simulations of the winter climate of the Laurentide Ice Sheet at the LGM. *Journal of Climate*, *17*(17), 3415–3433. https://doi.org/10.1175/1520-0442(2004)017<3415:PMSOTW>2.0.CO;2
Brunelle, B. G., Sigman, D. M., Cook, M. S., Keigwin, L. D., Haug, G. H., Plessen, B., et al. (2007). Evidence from diatom-bound nitrogen isotopes for subarctic Pacific stratification during the last ice age and a link to North Pacific denitrification changes. *Paleoceanography*, *22*, PA1215. https://doi.org/10.1029/2005PA001205
Brunelle, B. G., Sigman, D. M., Jaccard, S. L., Keigwin, L. D., Plessen, B., Schettler, G., et al. (2010). Glacial/interglacial changes in nutrient supply and stratification in the western subarctic North Pacific since the penultimate glacial maximum. *Quaternary Science Reviews*, *29*(19–20), 2579–2590. https://doi.org/10.1016/j.quascirev.2010.03.010
Caissie, B. E., Brigham-Grette, J., Lawrence, K. T., Herbert, T. D., & Cook, M. S. (2010). Last Glacial Maximum to Holocene sea surface conditions at Umnak Plateau, Bering Sea, as inferred from diatom, alkenone, and stable isotope records. *Paleoceanography*, *25*, PA1206. https://doi. org/10.1029/2008PA001671
Canfield, D. E. (1994). Factors influencing organic-carbon preservation in marine-sediments. *Chemical Geology*, *114*(3–4), 315–329. https://doi.org/10.1016/0009-2541(94)90061-2
Chase, Z., Anderson, R. F., Fleisher, M. Q., & Kubik, P. W. (2002). The influence of particle composition and particle flux on scavenging of Th, Pa and Be in the ocean. *Earth and Planetary Science Letters*, *204*, 215–229.
Chase, Z., Anderson, R. F., Fleisher, M. Q., & Kubik, P. W. (2003). Scavenging of ^{230}Th, ^{231}Pa and ^{10}Be in the Southern Ocean (SW Pacific sector): The importance of particle flux and advection. *Deep-Sea Research Part II: Topical Studies in Oceanography*, *50*, 739–768.
Cheng, H., Lawrence, E. R., Shen, C. C., Polyak, V. J., Asmerom, Y., Woodhead, J., et al. (2013). Improvements in ^{230}Th dating, ^{230}Th and ^{234}U half-life values, and U-Th isotopic measurements by multi-collector inductively coupled plasma mass spectrometry. *Earth and Planetary Science Letters*, *371–372*, 82–91. https://doi.org/10.1016/j.epsl.2013.04.006
COHMAP (1988). Climatic changes of the last 18,000 years: Observations and model simulations. *Science (80-.)*, *241*(4869), 1043–1052.
Cole, T. G. (1985). Composition, oxygen isotope geochemistry and origin of smectite in the metalliferous sediments of the Bauer Deep, southeast Pacific. *Geochimica et Cosmochimica Acta*, *49*(1), 221–235. https://doi.org/10.1016/0016-7037(85)90206-6
Cook, M. S., Keigwin, L. D., & Sancetta, C. A. (2005). The deglacial history of surface and intermediate water of the Bering Sea. *Deep Sea Research, Part II*, *52*, 2163–2173. https://doi.org/10.1016/j.dsr2.2005.07.004
Cook, M. S., Ravelo, A. C., Mix, A., Nesbitt, I. M., & Miller, N. V. (2016). Tracing subarctic Pacific water masses with benthic foraminiferal stable isotopes during the LGM and late Pleistocene. *Deep-Sea Research Part II: Topical Studies in Oceanography*, *125–126*, 84–95. https://doi.org/ 10.1016/j.dsr2.2016.02.006
Costa, K. M., Anderson, R. F., Mcmanus, J. F., Winckler, G., Middleton, J. L., & Langmuir, C. H. (2018). Trace element (Mn, Zn, Ni, V) and authi- genic uranium (aU) geochemistry reveal sedimentary redox history on the Juan de Fuca Ridge, North Pacific Ocean. *Geochimica et Cosmochimica Acta*, *236*, 79–98. https://doi.org/10.1016/j.gca.2018.02.016
Costa, K. M., Jacobel, A. W., McManus, J. F., Anderson, R. F., Winckler, G., & Thiagarajan, N. (2017). Productivity patterns in the Equatorial Pacific over the last 30,000 years. *Global Biogeochemical Cycles*, *31*, 850–865. https://doi.org/10.1002/2016GB005579
Costa, K. M., & McManus, J. F. (2017). Efficacy of ^{230}Th normalization in sediments from the Juan de Fuca Ridge, northeast Pacific Ocean. *Geochimica et Cosmochimica Acta*, *197*, 215–225. https://doi.org/10.1016/j.gca.2016.10.034 Costa, K. M., McManus, J. F., & Anderson, R. F. (2017). Radiocarbon and stable isotope evidence for changes in sediment mixing in the North Pacific over the past 30 kyr. *Radiocarbon*, 1–23. https://doi.org/10.1017/RDC.2017.91
Costa, K. M., McManus, J. F., Anderson, R. F., Ren, H., Sigman, D. M., Winckler, G., et al. (2016). No iron fertilization in the equatorial Pacific Ocean during the last ice age. *Nature*, *529*(7587), 519–522. https://doi.org/10.1038/nature16453
Costa, K. M., McManus, J. F., Boulahanis, B., Carbotte, S. M., Winckler, G., Huybers, P., & Langmuir, C. H. (2016). Sedimentation, stratigraphy and physical properties of sediment on the Juan de Fuca Ridge. *Marine Geology*, *380*, 163–173.
Davies, M. H., Mix, A. C., Stoner, J. S., Addison, J. A., Jaeger, J., Finney, B., & Wiest, J. (2011). The deglacial transition on the southeastern Alaska Margin: Meltwater input, sea level rise, marine productivity, and sedimentary anoxia. *Paleoceanography*, *26*, PA2223. https://doi.org/10.1029/2010PA002051
De Boer, A. M., & Nof, D. (2004). The Bering Strait's grip on the Northern Hemisphere climate. *Deep Sea Research Part A. Oceanographic Research Papers*, *51*(10), 1347–1366. https://doi.org/10.1016/j.dsr.2004.05.003
Dickens, G. R. (2001). Sulphate profiles and barium fronts in sediments on the Blake Ridge: Present and past methane fluxes through a large gas hydrate resevoir. *Geochimica et Cosmochimica Acta*, *65*(4), 529–543.
Dixit, S., Van Cappellen, P., & Van Bennekom, A. J. (2001). Processes controlling solubility of biogenic silica and pore water build-up of silicic acid in marine sediments. *Marine Chemistry*, *73*(3–4), 333–352. https://doi.org/10.1016/S0304-4203(00)00118-3
Dohonoe, A., & Battisti, D. S. (2009). Causes of reduced North Atlantic storm activity in a CAM3 simulation of the last glacial maximum. *Journal of Climate*, *22*(18), 4793–4808. https://doi.org/10.1175/2009JCLI2776.1
Dubois, N., Kienast, M., Kienast, S., Calvert, S. E., Franois, R., & Anderson, R. F. (2010). Sedimentary opal records in the eastern equatorial Pacific: It is not all about leakage. *Global Biogeochemical Cycles*, *24*, GB4020. https://doi.org/10.1029/2010GB003821
Dymond, J., Suess, E., & Lyle, M. W. (1992). Barium in deep-sea sediment: A geochemical proxy for paleoproductivity. *Paleoceanography*, *7*(2), 163–181. https://doi.org/10.1029/92PA00181
Eagle, M., Paytan, A., & Murray, R. W. (2003). A comparison between excess barium and barite as indicators of carbon export. *Paleoceanography*, *18*(1), 1021. https://doi.org/10.1029/2002PA000793
Emile-Geay, J., Cane, M. A., Naik, N., Seager, R., Clement, A. C., & van Geen, A. (2003). Warren revisited: Atmospheric freshwater fluxes and '"Why is no deep water formed in the North Pacific,"'. *Journal of Geophysical Research*, *108*(C6), 3178. https://doi.org/10.1029/2001JC001058

Farrell, J. W., & Prell, W. L. (1989). Climatic change and CaCO3 Preservation: An 800,000 year bathymetric reconstruction from the Central Equatorial Pacific Ocean. *Paleoceanography*, *4*, 447–466. https://doi.org/10.1029/PA004i004p00447

Fleisher, M. Q., & Anderson, R. F. (2003). Assessing the collection efficiency of Ross Sea sediment traps using ^{230}Th and ^{231}Pa. *Deep-Sea Research Part II: Topical Studies in Oceanography*, *50*, 693–712.

Fraile, I., Schulz, M., Mulitza, S., Merkel, U., Prange, M., & Paul, A. (2009). Modeling the seasonal distribution of planktonic foraminifera during the last glacial maximum. *Paleoceanography*, *24*, PA2216. https://doi.org/10.1029/2008PA001686

Francois, R., Altabet, M. A., Yu, E., Sigman, D. M., Bacon, M. P., Frank, M., et al. (1997). Contribution of Southern Ocean surface-water stratifi- cation to low atmospheric CO_2 concentrations during the last glacial period. *Nature*, *389*, 929–936.

Francois, R., Frank, M., van der Loeff, M. R., & Bacon, M. P. (2004). ^{230}Th normalization: An essential tool for interpreting sedimentary fluxes during the late Quaternary. *Paleoceanography*, *19*, PA1018. https://doi.org/10.1029/2003PA000939

Freeman, E., Skinner, L. C., Tisserand, A., Dokken, T., Timmermann, A., Menviel, L., & Friedrich, T. (2015). An Atlantic-Pacific ventilation seesaw across the last deglaciation. *Earth and Planetary Science Letters*, *424*, 237–244. https://doi.org/10.1016/j.epsl.2015.05.032

Galbraith, E. D., Jaccard, S. L., Pedersen, T. F., Sigman, D. M., Haug, G. H., Cook, M., et al. (2007). Carbon dioxide release from the North Pacific abyss during the last deglaciation. *Nature*, *449*(7164), 890–893. https://doi.org/10.1038/nature06227

Galbraith, E. D., Kienast, M., Jaccard, S. L., Pedersen, T. F., Brunelle, B. D., Sigman, D. M., & Kiefer, T. (2008). Consistent relationship between global climate and surface nitrate utilization in the western subarctic Pacific throughout the last 500 ka. *Paleoceanography*, *23*, PA2212. https://doi.org/10.1029/2007PA001518

Ganeshram, R. S., Calvert, S. E., Pedersen, T. F., & Cowie, G. L. (1999). Factors controlling the burial of organic carbon in laminated and bio-turbated sediments off NW Mexico: Implications for hydrocarbon preservation. *Geochimica et Cosmochimica Acta*, *63*(11–12), 1723–1734. https://doi.org/10.1016/S0016-7037(99)00073-3

Gargett, A. E. (1991). Physical processes and the maintenance of nutrient-rich euphotic zones. *Limnology and Oceanography*, *36*(8), 1527–1545. https://doi.org/10.4319/lo.1991.36.8.1527

Gebhardt, H., Sarnthein, M., Grootes, P. M., Kiefer, T., Kuehn, H., Schmieder, F., & Röhl, U. (2008). Paleonutrient and productivity records from the subarctic North Pacific for Pleistocene glacial terminations I to V. *Paleoceanography*, *23*, PA4212. https://doi.org/10.1029/2007PA001513 Geibert, W., & Usbeck, R. (2004). Adsorption of thorium and protactinium onto different particle types: Experimental findings. *Geochimica et Cosmochimica Acta*, *68*(7), 1489–1501. https://doi.org/10.1016/j.gca.2003.10.011

Glover, D. M., Wroblewski, J. S., & McClain, C. R. (1994). Dynamics of the transition zone in coastal zone color scanner-sensed ocean color in the North Pacific during oceanographic spring. *Journal of Geophysical Research*, *99*(C4), 7501. https://doi.org/10.1029/93JC02144

Gorbarenko, S. A. (1996). Stable isotope and lithologic evidence of late-glacial and Holocene oceanography of the Northwestern Pacific and its marginal seas. *Quaternary Research*, *250*, 230–250.

Gorbarenko, S. A., Southon, J. R., Keigwin, L. D., Cherepanova, M. V., & Gvozdeva, I. G. (2004). Late Pleistocene-Holocene oceanographic variability in the Okhotsk Sea: Geochemical, lithological and paleontological evidence. *Palaeogeography Palaeoclimatology Palaeoecology*, *209*(1–4), 281–301. https://doi.org/10.1016/j.palaeo.2004.02.013

Gray, W. R., Rae, J. W. B., Wills, R. C. J., Shevenell, A. E., Taylor, B., Burke, A., et al. (2018). Deglacial upwelling, productivity and CO_2 outgassing in the North Pacific Ocean. *Nature Geoscience*, *11*, 340–344. https://doi.org/10.1038/s41561-018-0108-6

Grigorov, I., Rigual-Hernandez, A. S., Honjo, S., Kemp, A. E. S., & Armand, L. K. (2014). Settling fluxes of diatoms to the interior of the Antarctic circumpolar current along 170°W. *Deep Sea Research Part I: Oceanographic Research Papers*, *93*, 1–13. https://doi.org/10.1016/j.dsr.2014.07.008

Harrison, P. J., Boyd, P. W., Varela, D. E., Takeda, S., Shiomoto, A., & Odate, T. (1999). Comparison of factors controlling phytoplankton pro- ductivity in the NE and NW subarctic Pacific gyres. *Progress in Oceanography*, *43*(2–4), 205–234. https://doi.org/10.1016/S0079-6611(99)00015-4

Hartnett, H. E., Keil, R. G., Hedges, J. I., & Devol, A. H. (1998). Influence of oxygen exposure time on organic carbon preservation in continental margin sediments. *Nature*, *391*(February), 572–575. https://doi.org/10.1038/35351

Haug, G. H., Ganopolski, A., Sigman, D. M., Rosell-mele, A., Swann, G. E. A., Tiedemann, R., et al. (2005). North Pacific seasonality and the glaciation of North America 2.7 million years ago. *Nature*, *433*, 821–825.

Haug, G. H., Sigman, D. M., Tiedemann, R., Pedersen, T. F., & Sarntheim, M. (1999). Onset of permanent stratifcation in the subarctic Pacific Ocean. *Nature*, *401*(October), 779–782.

Hayes, C. T., Anderson, R. F., Fleisher, M. Q., Serno, S., Winckler, G., & Gersonde, R. (2014). Biogeography in ^{231}Pa/^{230}Th ratios and a balanced ^{231}Pa budget for the Pacific Ocean. *Earth and Planetary Science Letters*, *391*, 307–318. https://doi.org/10.1016/j.epsl.2014.02.001

Hayes, C. T., Anderson, R. F., Jaccard, S. L., François, R., Fleisher, M. Q., Soon, M., & Gersonde, R. (2013). A new perspective on boundary scavenging in the North Pacific Ocean. *Earth and Planetary Science Letters*, *369–370*, 86–97. https://doi.org/10.1016/j.epsl.2013.03.008

Hedges, J. I., Hu, F. S., Devol, A. H., Hartnett, H. E., Tsamakis, E., & Keil, R. G. (1999). Sedimentary organic matter preservation: A test for selective degradation under oxic conditions. *American Journal of Science*, *299*(7–9), 529–555. https://doi.org/10.2475/ajs.299.7-9.529

Henderson, G. M., & Anderson, R. F. (2003). The U-series toolbox for paleoceanography. *Reviews in Mineralogy and Geochemistry*, *52*, 493–531.

Henderson, G. M., Heinze, C., Anderson, R. F., & Winguth, A. M. E. (1999). Global distribution of the $_{230}$Th flux to ocean sediments constrained by GCM modelling. *Deep Sea Research Part I: Oceanographic Research Papers*, *46*, 1861–1893. https://doi.org/10.1016/S0967- 0637(99)00030-8

Hendy, I. L., & Cosma, T. (2008). Vulnerability of the Cordilleran Ice Sheet to iceberg calving during late quaternary rapid climate change events. *Paleoceanography*, *23*, PA2101. https://doi.org/10.1029/2008PA001606

Henry, L. G., McManus, J. F., Curry, W. B., Roberts, N. L., Piotrowski, A. M., & Keigwin, L. D. (2016). North Atlantic ocean circulation and abrupt climate change during the last glaciation. *Science*, *353*(6298), 470–474.

Hernandez-Sanchez, M. T., Mills, R. A., Planquette, H., Pancost, R. D., Hepburn, L., Salter, I., & Fitzgeorge-balfour, T. (2011). Quantifying export production in the Southern Ocean: Implications for the Ba xs proxy. *Paleoceanography*, *26*, PA4222. https://doi.org/10.1029/2010PA002111 Hillaire-Marcel, C., & de Vernal, A. (2008). Stable isotope clue to episodic sea ice formation in the glacial North Atlantic. *Earth and Planetary Science Letters*, *268*(1–2), 143–150. https://doi.org/10.1016/j.epsl.2008.01.012

Honda, M. C., Imai, K., Nojiri, Y., Hoshi, F., Sugawara, T., & Kusakabe, M. (2002). The biological pump in the northwestern North Pacific based on fluxes and major components of particulate matter obtained by sediemnt-trap experiemnts (1997–2000). *Deep Sea Research Part II: Topical Studies in Oceanography*, *49*, 5595–5625.

Hönisch, B., Allen, K. A., Lea, D. W., Spero, H. J., Eggins, S. M., Arbuszewski, J., et al. (2013). The influence of salinity on Mg/Ca in planktic foraminifers—Evidence from cultures, core-top sediments and complementary δ18O. *Geochimica et Cosmochimica Acta*, *121*, 196–213. https://doi.org/10.1016/j.gca.2013.07.028

Horikawa, K., Asahara, Y., Yamamoto, K., & Okazaki, Y. (2010). Intermediate water formation in the Bering Sea during glacial periods: Evidence from neodymium isotope ratios. *Geology*, *38*(5), 435–438.

Hu, A., Meehl, G. A., Han, W., Abe-Ouchi, A., Morrill, C., Okazaki, Y., & Chikamoto, M. O. (2012). The Pacific-Atlantic seesaw and the Bering Strait.
Geophysical Research Letters, *39*, L03702. https://doi.org/10.1029/2011GL050567

Hu, A., Meehl, G. A., Han, W., Otto-Bliestner, B., Abe-Ouchi, A., & Rosenbloom, N. (2015). Effects of the Bering Strait closure on AMOC and global climate under different background climates. *Progress in Oceanography*, *132*, 174–196. https://doi.org/10.1016/j. pocean.2014.02.004

Hu, A., Meehl, G. A., Otto-Bliesner, B. L., Waelbroeck, C., Han, W., Loutre, M. F., et al. (2010). Influence of Bering Strait flow and North Atlantic circulation on glacial sea-level changes. *Nature Geoscience*, *3*(2), 118–121. https://doi.org/10.1038/ngeo729

Hu, A., Meehl, G. A., Han, W., Timmermann, A., Otto-Bliesner, B., Liu, Z., et al. (2012). Role of the Bering Strait on the hysteresis of the ocean conveyor belt circulation and glacial climate stability. *Proceedings of the National Academy of Sciences*, *109*(17), 6417–6422. https:// doi.org/ 10.1073/pnas.1116014109

Iwasaki, S., Kimoto, K., Kuroyanagi, A., & Kawahata, H. (2017). Horizontal and vertical distributions of planktic foraminifera in the subarctic Pacific. *Marine Micropaleontology*, *130*, 1–14. https://doi.org/10.1016/j.marmicro.2016.12.001

Jaccard, S. L., Galbraith, E. D., Sigman, D. M., & Haug, G. H. (2010). A pervasive link between Antarctic ice core and subarctic Pacific sediment records over the past 800 kyrs. *Quaternary Science Reviews*, *29*(1–2), 206–212. https://doi.org/10.1016/j.quascirev.2009.10.007

Jaccard, S. L., Galbraith, E. D., Sigman, D. M., Haug, G. H., Francois, R., Pedersen, T. F., et al. (2009). Subarctic Pacific evidence for a glacial deepening of the oceanic respired carbon pool. *Earth and Planetary Science Letters*, *277*(1–2), 156–165. https://doi.org/10.1016/j. epsl.2008.10.017

Jaccard, S. L., Haug, G. H., Sigman, D. M., Pedersen, T. F., Thierstein, H. R., & Rohl, U. (2005). Glacial/interglacial changes in Subarctic North Pacific stratification. *Science*, *308*(5724), 1003–1006. https://doi.org/10.1126/science.1108696

Jang, K., Huh, Y., & Han, Y. (2017). Authigenic Nd isotope record of North Pacific Intermediate Water formation and boundary exchange on the Bering Slope. *Quaternary Science Reviews*, *156*, 150–163. https://doi.org/10.1016/j.quascirev.2016.11.032

Jonkers, L., Zahn, R., Thomas, A., Henderson, G., Abouchami, W., François, R., et al. (2015). Deep circulation changes in the central South Atlantic during the past 145 kyrs reflected in a combined $^{231}Pa/^{230}Th$, Neodymium isotope and benthic d13C record. *Earth and Planetary Science Letters*, *419*, 14–21. https://doi.org/10.1016/j.epsl.2015.03.004

Karlin, R., Lyle, M., & Heath, G. R. (1987). Authigenic magnetite formation in suboxic marine sediments. *Nature*, *326*(6112), 490–493. https:// doi.org/10.1038/326490a0

Katsuki, K., & Takahashi, K. (2005). Diatoms as paleoenvironmental proxies for seasonal productivity, sea-ice and surface circulation in the Bering Sea during the late Quaternary. *Deep-Sea Research Part II: Topical Studies in Oceanography*, *52*(16–18), 2110–2130. https://doi.org/ 10.1016/j.dsr2.2005.07.001

Kawakami, H., Honda, M. C., Wakita, M., & Watanabe, S. (2007). Time-series observation of dissolved inorganic carbon and nutrients in the northwestern North Pacific. *Journal of Oceanography*, *63*(6), 967–982. https://doi.org/10.1007/s10872-007-0081-y

Keigwin, L. D. (1987). North Pacific deep water formation during the latest glaciation. *Nature*, *330*, 362–364.

Keigwin, L. D. (1998). Glacial-age hydrography of the far northwest Pacific Ocean. *Paleoceanography*, *13*(4), 323–339. https://doi.org/10.1029/ 98PA00874

Keigwin, L. D., & Cook, M. S. (2007). A role for North Pacific salinity in stabilizing North Atlantic climate. *Paleoceanography*, *22*, PA3102. https:// doi.org/10.1029/2007PA001420

Keigwin, L. D., Jones, G. A., & Froelich, P. N. (1992). A 15,000 year paleoenvironmental record from Meiji Seamount, far northwestern Pacific. *Earth and Planetary Science Letters*, *111*, 425–440.

Keil, R. G., & Hedges, J. I. (1993). Sorption of organic matter to mineral surfaces and the preservation of organic matter in coastal marine sediments. *Chemical Geology*, *107*(3–4), 385–388. https://doi.org/10.1016/0009-2541(93)90215-5

Keil, R. G., Montlucon, D. B., Prahl, F. G., & Hedges, J. I. (1994). Sorptive preservation of labile organic matter in marine sediments. *Nature*, *370*, 549–552.

Kienast, S. S. (2003). *Palaeoceanography of the mid-latitude North East Pacific during the late Pleistocene*. Vancouver: The University of British Columbia.

Kienast, S. S., Hendy, I. L., Crusius, J., Pedersen, T. F., & Calvert, S. E. (2004). Export production in the subarctic North Pacific over the last 800 kyrs: No evidence for iron fertilization? *Journal of Oceanography*, *60*(3), 189–203. https://doi.org/10.1023/B:JOCE.0000038326.73943.aa

Kienast, S. S., Kienast, M., Mix, A. C., Calvert, S. E., & François, R. (2007). Thorium-230 normalized particle flux and sediment focusing in the
Panama Basin region during the last 30,000 years. *Paleoceanography*, *22*, PA2213. https://doi.org/10.1029/2006PA001357

Kirby, M. E., Feakins, S. J., Bonuso, N., Fantozzi, J. M., & Hiner, C. A. (2013). Latest Pleistocene to Holocene hydroclimates from Lake Elsinore, California. *Quaternary Science Reviews*, *76*, 1–15. https://doi.org/10.1016/j.quascirev.2013.05.023

Knudson, K. P., & Ravelo, A. C. (2015a). Enhanced subarctic Pacific Stratification and nutrient utilization during glacials over the last 1.2 Myr. *Geophysical Research Letters*, *42*, 9870–9879. https://doi.org/10.1002/2013GL058489.Received

Knudson, K. P., & Ravelo, A. C. (2015b). North Pacific Intermediate Water circulation enhanced by the closure of the Bering Strait. *Paleoceanography*, *30*, 1–18. https://doi.org/10.1002/2015PA002840.Received

Kohfeld, K. E., & Chase, Z. (2011). Controls on deglacial changes in biogenic fluxes in the North Pacific Ocean. *Quaternary Science Reviews*, *30*(23–24), 3350–3363. https://doi.org/10.1016/j.quascirev.2011.08.007

Kretschmer, S., Geibert, W., Rutgers van der Loeff, M. M., Schnabel, C., Xu, S., & Mollenhauer, G. (2011). Fractionation of ^{230}Th, ^{231}Pa, and ^{10}Be induced by particle size and composition within an opal-rich sediment of the Atlantic Southern Ocean. *Geochimica et Cosmochimica Acta*, *75*(22), 6971–6987. https://doi.org/10.1016/j.gca.2011.09.012

Kroopnick, P. M. (1985). The distribution of ^{13}C of CO_2 in the world oceans. *Deep Sea Research*, *32*, 57–84.

Kumar, P. K., Band, S. T., Ramesh, R., & Awasthi, N. (2018). Monsoon variability and upper ocean stratification during the last ~66 ka over the
Andaman Sea: Inferences from the δ18O records of planktonic foraminifera. *Quaternary International*, *479*(March), 12–18. https://doi.org/ 10.1016/j.quaint.2018.03.025

Kuroyanagi, A., Kawahata, H., Nishi, H., & Honda, M. C. (2008). Seasonal to interannual changes in planktonic foraminiferal assemblages in the northwestern North Pacific: Sediment trap results encompassing a warm period related to El Niño. *Palaeogeography Palaeoclimatology Palaeoecology*, *262*(1–2), 107–127. https://doi.org/10.1016/j.palaeo.2008.02.012

Lam, P. J., Robinson, L. F., Blusztajn, J., Li, C., Cook, M. S., McManus, J. F., & Keigwin, L. D. (2013). Transient stratification as the cause of the North Pacific productivity spike during deglaciation. *Nature Geoscience*, *6*(8), 622–626. https://doi.org/10.1038/ngeo1873

Li, C., & Battisti, D. S. (2008). Reduced Atlantic storminess during last glacial maximum: Evidence from a coupled climate model. *Journal of Climate*, *21*(14), 3561–3579. https://doi.org/10.1175/2007JCLI2166.1

Lisiecki, L. E., & Raymo, M. E. (2005). A Pliocene-Pleistocene stack of 57 globally distributed benthic d18O records. *Paleoceanography*, *20*, PA1003. https://doi.org/10.1029/2004PA001071

Lora, J. M., Mitchell, J. L., Risi, C., & Tripati, A. E. (2017). North Pacific atmospheric rivers and their influence on western North America at the Last Glacial Maximum. *Geophysical Research Letters*, *44*, 1051–1059. https://doi.org/10.1002/2016GL071541

Lynch-Stieglitz, J., Adkins, J. F., Curry, W. B., Dokken, T., Hall, I. R., Herguera, J. C., et al. (2007). Atlantic meridional overturning circulation during the Last Glacial Maximum. *Science*, *316*(5821), 66–69. https://doi.org/10.1126/science.1137127

Mackenzie, F. T., & Kump, L. R. (1995). Reverse weathering, clay mineral formation, and oceanic element cycles. *Science*, *270*(5236), 586–586. https://doi.org/10.1126/science.270.5236.586

Martin, J. H., & Fitzwater, S. E. (1988). Iron deficiency limits phyto-plankton growth in the northeast Pacific subarctic. *Nature*, *331*, 341–343.

Matsumoto, K., Oba, T., Lynch-Stieglitz, J., & Yamamoto, H. (2002). Interior hydrography and circulation of the glacial Pacific Ocean. *Quaternary Science Reviews*, *21*(14–15), 1693–1704. https://doi.org/10.1016/S0277-3791(01)00142-1 Matul, A. G. (2017). Probable limits of sea ice extent in the northwestern Subarctic Pacific during the last glacial maximum. *Oceanology*, *57*(5), 700–706. https://doi.org/10.1134/S0001437017050113

Max, L., Rippert, N., Lembke-Jene, L., Mackensen, A., Nurnberg, D., & Tiedemann, R. (2017). Evidence for enhanced convection of North Pacific Intermediate Water to the low-latitude Pacific under glacial conditions. *Paleoceanography*, *32*, 41–55. https://doi.org/10.1002/2016PA002994

McDonald, D., Pedersen, T. F., & Crusius, J. (1999). Multiple late Quaternary episodes of exceptional diatom production in the Gulf of Alaska. *Deep Sea Research, Part II*, *46*, 2993–3017. McGee, D., Broecker, W. S., & Winckler, G. (2010). Gustiness: The driver of glacial dustiness? *Quaternary Science Reviews*, *29*(17–18), 2340–2350. https://doi.org/10.1016/j.quascirev.2010.06.009

McManus, J., Berelson, W. M., Klinkhammer, G. P., Kilgore, T. E., & Hammond, D. E. (1994). Remobilization of barium in continental margin sediments. *Geochimica et Cosmochimica Acta*, *58*(22), 4899–4907. https://doi.org/10.1016/0016-7037(94)90220-8

McManus, J., Berelson, W. M., Klinkhammer, G. P., Johnson, K. S., Coale, K. H., Anderson, R. F., et al. (1998). Geochemistry of barium in marine sediments: Implications for its use as a paleoproxy. *Geochimica et Cosmochimica Acta*, *62*(21–22), 3453–3473. https://doi.org/10.1016/ S0016-7037(98)00248-8

McManus, J. F., Francois, R., Gherardi, J.-M., Keigwin, L. D., & Brown-Leger, S. (2004). Collapse and rapid resumption of Atlantic meridional circulation linked to deglacial climate changes. *Nature*, *428*(6985), 834–837. https://doi.org/10.1038/nature02494

Méheust, M., Stein, R., Fahl, K., & Gersonde, R. (2018). Sea-ice variability in the subarctic North Pacific and adjacent Bering Sea during the past 25 ka: New insights from IP25 and Uk'37 proxy records. *arktos*, *4*(8). https://doi.org/10.1007/s41063-018-0043-1

Menviel, L., Yu, J., Joos, F., Mouchet, A., Meissner, K. J., & England, M. H. (2017). Poorly ventilated deep ocean at the Last Glacial Maximum inferred from carbon isotopes A data-model comparison study. *Paleoceanography*, *32*, 2–17. https://doi.org/10.1002/2016PA003024

Michalopoulos, P., Aller, R. C., & Reeder, R. J. (2000). Conversion of diatoms to clays during early diagenesis in tropical, continental shell muds. *Geology*, *28*(12), 1095–1098. https://doi.org/10.1130/0091-7613(2000)28<1095:CODTCD>2.0.CO

Mikolajewicz, U., Crowley, T. J., Schiller, A., & Voss, R. (1997). Modelling teleconnections between the North Atlantic and North Pacific during the Younger Dryas. *Nature*, *387*, 384–387.

Mortlock, R. A., Charles, C. D., Froelich, P. N., Zibello, M. A., Saltzman, J., Hays, J. D., & Burckle, L. H. (1991). Evidence for lower productivity in the Antarctic Ocean during the last glaciation. *Nature*, *351*(6323), 220–223. https://doi.org/10.1038/351220a0

Mortlock, R. A., & Froelich, P. N. (1989). A simple method for the rapid determination of biogenic opal in pelagic marine sediments. *Deep Sea Research*, *36*(9), 1415–1426.

Müller, P. J., & Suess, E. (1979). Productivity, sedimentation rate, and sedimentary organic matter in the oceans-I. Organic carbon preserva- tion. *Deep Sea Research Part A. Oceanographic Research Papers*, *26*(12), 1347–1362. https://doi.org/10.1016/0198-0149(79)90003-7

Murray, R. W., Leinen, M., & Knowlton, C. W. (2012). Links between iron input and opal deposition in the Pleistocene equatorial Pacific Ocean. *Nature Geoscience*, *5*(4), 270–274. https://doi.org/10.1038/ngeo1422 Murray, R. W., Miller, D. J., & Kryc, K. A. (2000). Analysis of major and trace elements in rocks, sediments, and interstitial waters by inductively coupled plasma-atomic emission spectrometry (ICP-AES), *ODP Tech. Note*.

Narita, H., Sato, M., Tsunogai, S., Murayama, M., & Harada, N. (2002). Biogenic opal indicating less productive northwestern. *North Pacific During the Glacial Ages*, *29*(15), 2–5.

Nelson, D. M., Treguer, P., Brzezinski, M. A., Leynaert, A., & Queguiner, B. (1995). Production and dissolution of biogenic silica in the ocean: Revised global estimates, comparison with regional data and relationship to biogenic sedimentation. *Global Biogeochemical Cycles*, *9*(3), 359–372. https://doi.org/10.1029/95GB01070

Ng, H. C., Robinson, L. F., Mcmanus, J. F., Mohamed, K. J., Jacobel, A. W., Ivanovic, R. F., et al. (2018). Coherent deglacial changes in western Atlantic Ocean circulation. *Nature Communications*, *9*, 2947. https://doi.org/10.1038/s41467-018-05312-3

Nozaki, Y., Horibe, Y., & Tsubota, H. (1981). The water column distributions of thorium isotopes in the western North Pacific. *Earth and Planetary Science Letters*, *54*, 203–216. https://doi.org/10.1016/0012-821X(81)90004-2

Oba, T., Irino, T., Yamamoto, M., Murayama, M., Takamura, A., & Aoki, K. (2006). Paleoceanographic change off central Japan since the last 144,000 years based on high-resolution oxygen and carbon isotope records. *Global and Planetary Change*, *53*(1–2), 5–20. https://doi.org/10.1016/j.gloplacha.2006.05.002

O'Gorman, P. A. (2010). Understanding the varied response of the extratropical storm tracks to climate change. *Proceedings of the National Academy of Sciences*, *107*(45), 19,176–19,180. https://doi.org/10.1073/pnas.1011547107

Okazaki, Y., Takahashi, K., Asahi, H., Katsuki, K., Hori, J., Yasuda, H., et al. (2005). Productivity changes in the Bering Sea during the late Quaternary. *Deep-Sea Research Part II: Topical Studies in Oceanography*, *52*(16–18), 2150–2162. https://doi.org/10.1016/ j.dsr2.2005.07.003

Okazaki, Y., Takahashi, K., Katsuki, K., Ono, A., Hori, J., Sakamoto, T., et al. (2005). Late Quaternary paleoceanographic changes in the south-western Okhotsk Sea: Evidence from geochemical, radiolarian, and diatom records. *Deep-Sea Research Part II: Topical Studies in Oceanography*, *52*(16–18), 2332–2350. https://doi.org/10.1016/j.dsr2.2005.07.007

Okazaki, Y., Timmermann, A., Menviel, L., Harada, N., Abe-Ouchi, A., Chikamoto, M. O., et al. (2010). Deepwater formation in the North Pacific during the Last Glacial termination. *Science*, *329*(5988), 200–204.

O'Neil, J. R. (1968). Hydrogen and oxygen isotope fractionation between ice and water. *The Journal of Physical Chemistry*, *72*, 3683–3684.

Oster, J. L., Ibarra, D. E., Winnick, M. J., & Maher, K. (2015). Steering of westerly storms over western North America at the Last Glacial Maximum. *Nature Geoscience*, *8*(3), 201–205. https://doi.org/10.1038/ngeo2365

Owens, S. A., Buesseler, K. O., & Sims, K. W. W. (2011). Re-evaluating the ^{238}U-salinity relationship in seawater: Implications for the ^{238}U–^{234}Th disequilibrium method. *Marine Chemistry*, *127*(1–4), 31–39. https://doi.org/10.1016/j.marchem.2011.07.005

Parker, A. O., Schmidt, M. W., & Chang, P. (2015). Tropical North Atlantic subsurface warming events as a fingerprint for AMOC variability during Marine Isotope Stage 3. *Paleoceanography*, *30*, 1425–1436. https://doi.org/10.1002/2015PA002832.Received

Paytan, A., & Griffith, E. M. (2007). Marine barite: Recorder of variations in ocean export productivity. *Deep-Sea Research Part II: Topical Studies in Oceanography*, *54*(5–7), 687–705. https://doi.org/10.1016/j.dsr2.2007.01.007

Pease, C. H. (1980). Eastern Bering Sea ice processes. *Monthly Weather Review*, *108*(12), 2015–2023. https://doi.org/10.1175/1520-0493(1980)108<2015:EBSIP>2.0.CO;2

Penny, S. M., Battisti, D. S., & Gerard, H. R. (2013). Examining mechanisms of variability within the Pacific storm track: Upstream seeding and jet-core strength. *Journal of Climate*, *26*(14), 5242–5259. https://doi.org/10.1175/JCLI-D-12-00017.1

Pichat, S., Sims, K. W. W., Francois, R., McManus, J. F., Brown-Leger, S., & Albarede, F. (2004). Lower export production during glacial periods in
the equatorial Pacific derived from (231Pa/230Th)xs,0 measurements in deep-sea sediments. *Paleoceanography*, *19*, PA4023. https://doi. org/10.1029/2003PA000994

Praetorius, S. K., McManus, J. F., Oppo, D. W., & Curry, W. B. (2008). Episodic reductions in bottom-water currents since the last ice age. *Nature Geoscience*, *1*(7), 449–452. https://doi.org/10.1038/ngeo227

Ragueneau, O., Tréguer, P., Leynaert, A., Anderson, R. F., Brzezinski, M. A., DeMaster, D. J., et al. (2000). A review of the Si cycle in the modern ocean: Recent progress and missing gaps in the application of biogenic opal as a paleoproductivity proxy. *Global and Planetary Change*, *26*(4), 317–365. https://doi.org/10.1016/S0921-8181(00)00052-7

Rahman, S., Aller, R. C., & Cochran, J. K. (2016). Cosmogenic 32Si as a tracer of biogenic silica burial and diagenesis: Major deltaic sinks in the silica cycle. *Geophysical Research Letters*, *43*, 7124–7132. https://doi.org/10.1002/2016GL069929

Reid, J. L. (1962). On circulation, phosphate-phosphorus content, and zooplankton volumes in the upper part of the Pacific Ocean. *Limnology and Oceanography*, *7*, 287–306.

Ren, H., Studer, A. S., Serno, S., Sigman, D. M., Winckler, G., Anderson, R. F., et al. (2015). Glacial-to-interglacial changes in nitrate supply and consumption in the subarctic North Pacific from microfossil-bound N isotopes at two trophic levels. *Paleoceanography*, *30*, 1217–1232. https://doi.org/10.1002/2014PA002765

Reynolds, L., & Thunell, R. C. (1985). Seasonal succession of planktonic foraminifera in the subpolar North Pacific. *Journal of Foraminiferal Research*, *15*(4), 282–301. https://doi.org/10.2113/gsjfr.15.4.282

Riethdorf, J. R., Max, L., Nürnberg, D., Lembke-Jene, L., & Tiedemann, R. (2013). Deglacial development of (sub) sea surface temperature and salinity in the subarctic northwest Pacific: Implications for upper-ocean stratification. *Paleoceanography*, *28*, 91–104. https://doi.org/10.1002/palo.20014

Riethdorf, J.-R., Nurnberg, D., Max, L., Tiedemann, R., Gorbarenko, S. A., & Malakhov, M. I. (2013). Millennial-scale variability of marine pro- ductivity and terrigenous matter supply in the western Bering Sea over the past 180kyr. *Climate of the Past*, *9*, 1345–1373. https://doi.org/ 10.5194/cp-9-1345-2013

Rind, D. H. (1998). Latitudinal temperature gradients and climate change. *Journal of Geophysical Research*, *103*(D6), 5943. https://doi.org/10.1029/97JD03649

Riviere, G., Berthou, S., Lapeyre, G., & Kageyama, M. (2018). On the reduced North Atlantic storminess during the last glacial period: The role of topography in shaping synoptic eddies. *Journal of Climate*, *31*(4), 1637–1652.

Robinson, R. S., Brunelle, B. G., & Sigman, D. M. (2004). Revisiting nutrient utilization in the glacial Antarctic: Evidence from a new method for diatom-bound N isotopic analysis. *Paleoceanography*, *19*, PA3001. https://doi.org/10.1029/2003PA000996

Sakamoto, T., Ikehara, M., Aoki, K., Iijima, K., Kimura, N., Nakatsuka, T., & Wakatsuchi, M. (2005). Ice-rafted debris (IRD)-based sea-ice expansion events during the past 100 kyrs in the Okhotsk Sea. *Deep-Sea Research Part II: Topical Studies in Oceanography*, *52*(16–18), 2275–2301. https://doi.org/10.1016/j.dsr2.2005.08.007

Sancetta, C. (1983). Effect of Pleistocene glaciation upon oceanographic characteristics of the North Pacific Ocean and Bering Sea. *Deep Sea Research Part A. Oceanographic Research Papers*, *30*(8), 851–869. https://doi.org/10.1016/0198-0149(83)90004-3

Sasaoka, K., Saitoh, S., Asanuma, I., Imai, K., Honda, M. C., Nojiri, Y., & Saino, T. (2002). Temporal and spatial variability of chlorophyll a in the subarctic northwestern Pacific determined from satellite and ship observations during 1997–1999. *Deep-Sea Research Part II: Topical Studies in Oceanography*, *49*(24–25), 5557–5576.

Sato, M., Narita, H., & Tsunogai, S. (2002). Barium increasing prior to opal during the last termination of glacial ages in the Okhotsk Sea sediments. *Journal of Oceanography*, *58*, 461–467.

Schenau, S. J., Prins, M. A., De Lange, G. J., & Monnin, C. (2001). Barium accumulation in the Arabian Sea: Controls on barite preservation in marine sediments. *Geochimica et Cosmochimica Acta*, *65*(10), 1545–1556. https://doi.org/10.1016/S0016-7037(01)00547-6

Seki, O., Ikehara, M., Kawamura, K., Nakatsuka, T., Ohnishi, K., Wakatsuchi, M., et al. (2004). Reconstruction of paleoproductivity in the Sea of Okhotsk over the last 30 kyr. *Paleoceanography*, *19*, PA1016. https://doi.org/10.1029/2002PA000808

Serno, S., Winckler, G., Anderson, R. F., Hayes, C. T., Ren, H., Gersonde, R., & Haug, G. H. (2014). Using the natural spatial pattern of marine productivity in the Subarctic North Pacific to evaluate paleoproductivity proxies. *Paleoceanography*, *29*, 438–453. https://doi.org/10.1002/2013PA002594.Received

Serno, S., Winckler, G., Anderson, R. F., Jaccard, S. L., Kienast, S. S., & Haug, G. H. (2017). Change in dust seasonality as the primary driver for orbital-scale dust storm variability in East Asia. *Geophysical Research Letters*, *44*, 3796–3805. https://doi.org/10.1002/2016GL072345

Serno, S., Winckler, G., Anderson, R. F., Maier, E., Ren, H., Gersonde, R., & Haug, G. H. (2015). Comparing dust flux records from the Subarctic North Pacific and Greenland: Implications for atmospheric transport to Greenland and for the application of dust as a chronostratigraphic tool. *Paleoceanography*, *30*, 583–600. https://doi.org/10.1002/2014PA002748

Shaffer, G., & Bendtsen, J. (1994). Role of the Bering Strait in controlling North Atlantic Ocean circulation and climate. *Nature*, *367*(6461), 354–357. https://doi.org/10.1038/367354a0

Shcherbina, A. Y., Talley, L. D., & Rudnick, D. L. (2003). Direct observations of North Pacific ventilation: Brine rejection in the Okhotsk Sea. *Science (80-.)*, *302*(5652), 1952–1955. https://doi.org/10.1126/science.1088692

Shigemitsu, M., Narita, H., Watanabe, Y. W., Harada, N., & Tsunogai, S. (2007). Ba, Si, U, Al, Sc, La, Th, C and $^{13}C/^{12}C$ in a sediment core in the western subarctic Pacific as proxies of past biological production. *Marine Chemistry*, *106*(3–4), 442–455. https://doi.org/10.1016/j.marchem.2007.04.004

Sigman, D. M., Jaccard, S. L., & Haug, G. H. (2004). Polar Ocean stratification in a cold climate. *Nature*, *428*, 59–63.

Sillen, L. G. (1961). The physical chemistry of seawater. In *Oceanography* (pp. 549–581). Washington, DC: American Association for the Advancement of Science.

Smith, J. N., Brown, R. M., Williams, W. J., Robert, M., Nelson, R., & Moran, S. B. (2015). Arrival of the Fukushima radioactivity plume in North American continental waters. *Proceedings of the National Academy of Sciences*, *112*(5), 1310–1315. https://doi.org/10.1073/pnas.1412814112

Tabata, S. (1975). The general circulation of the Pacific Ocean and a brief account of the oceanographic structure of the North Pacific Ocean: Part I—Circulation and volume transports. *Atmosphere (Basel)*, *13*(4), 133–168. https://doi.org/10.1080/00046973.1976.9648398

Talley, L. D. (1993). Distribution and formation of North Pacific Intermediate Water. *American Meteorological Society*, *23*, 517–537.

Talley, L. D. (2008). Freshwater transport estimates and the global overturning circulation: Shallow, deep and throughflow components. *Progress in Oceanography*, *78*(4), 257–303.

https://doi.org/10.1016/j.pocean.2008.05.001 Taylor, B. J., Rae, J. W. B., Gray, W. R., Darling, K. F., Burke, A., Gersonde, R., et al. (2018).

Distribution and ecology of planktic foraminifera in the North Pacific: Implications for paleo-reconstructions. *Quaternary Science Reviews*, *191*, 256–274. https://doi.org/10.1016/j.quascirev.2018.05.006

Taylor, S. R., & McLennan, S. M. (1995). The geochemical evolution of the continental crust. *Reviews of Geophysics*, *33*(95), 241–265. https://doi. org/10.1029/95RG00262

Thomson, R. E. (1981). *Oceanography of the British Columbia Coast*. Ottawa: Canadian Special Publication of Fisheries and Aquatic Sciences, National Research Council.

Torres, M. E., Brumsack, H. J., Bohrmann, G., & Emeis, K.-C. (1996). Barite fronts in continental margin sediments: A new look at barium remobilization in the zone of sulfate reduction and formation of heavy barites in diagenetic fronts. *Chemical Geology*, *127*(1–3), 125–139.

Treguer, P. J., & de la Rocha, C. L. (2013). The World Ocean silica cycle. *Annual Review of Marine Science*, *5*, 477–501. https://doi.org/10.1146/ annurev-marine-121211-172346

Tsuda, A., Kiyosawa, H., Kuwata, A., Mochizuki, M., Shiga, N., Saito, H., et al. (2005). Responses of diatoms to iron-enrichment (SEEDS) in the western subarctic Pacific, temporal and spatial comparisons. *Progress in Oceanography*, *64*(2–4), 189–205. https://doi.org/10.1016/j.pocean.2005.02.008

Van Cappellen, P., & Qiu, L. (1997). Biogenic silica dissolution in sediments of the Southern Ocean. II. Kinetics. *Deep-Sea Research Part II: Topical Studies in Oceanography*, *44*(5), 1129–1149. https://doi.org/10.1016/S0967-0645(96)00113-0

van Os, B. J., Middelburg, J. J., & de Lange, G. J. (1991). Possible diagenetic mobilization of barium in sapropelic sediment from the eastern Mediterranean. *Marine Geology*, *100*(1–4), 125–136.

Wara, M. W., Ravelo, A. C., & Delaney, M. L. (2005). Permanent El Nino-like conditions during the Pliocene warm period. *Science*, *309*, 758–761. Warren, B. A. (1983). Why is no deep water formed in the North Pacific? *Journal of Marine Research*, *41*(2), 327–347.

https://doi.org/10.1357/002224083788520207

Wheeler, P. A., Huyer, A., & Fleischbein, J. (2003). Cold halocline, increased nutrients and higher chlorophyll off Oregon in 2002. *Geophysical Research Letters*, *30*(15), 8021. https://doi.org/10.1029/2003GL017395

Whitney, F. A. (2011). Nutrient variability in the mixed layer of the subarctic Pacific Ocean, 1987–2010. *Journal of Oceanography*, *67*(4), 481–492. https://doi.org/10.1007/s10872-011-0051-2

Whitney, F. A., Crawford, W. R., & Harrison, P. J. (2005). Physical processes that enhance nutrient transport and primary productivity in the coastal and open ocean of the subarctic NE Pacific. *Deep-Sea Research Part II: Topical Studies in Oceanography*, *52*(5–6), 681–706. https:// doi.org/10.1016/j.dsr2.2004.12.023

Whitney, F. A., & Freeland, H. J. (1999). Variability in upper-ocean water properties in the NE Pacific Ocean. *Deep-Sea Research Part II: Topical Studies in Oceanography*, *46*, 2351–2370.

Winckler, G., Anderson, R. F., Fleisher, M. Q., McGee, D., & Mahowald, N. (2008). Covariant glacial-interglacial dust fluxes in the equatorial Pacific and Antarctica. *Science*, *320*(5872), 93–96. https://doi.org/10.1126/science.1150595

Winckler, G., Anderson, R. F., Jaccard, S. L., & Marcantonio, F. (2016). Ocean dynamics, not dust, have controlled equatorial Pacific productivity over the past 500,000 years. *Proceedings of the National Academy of Sciences*, *113*(22), 6119–6124. https://doi.org/10.1073/pnas.1600616113

Wong, C. S., Waser, N. A. D., Nojiri, Y., Whitney, F. A., Page, J. S., & Zeng, J. (2002). Seasonal cycles of nutrients and dissolved inorganic carbon at high and mid latitudes in the North Pacific Ocean during the Skaugran cruises: Determination of new production and nutrient uptake ratios. *Deep-Sea Research Part II: Topical Studies in Oceanography*, *49*(24–25), 5317–5338. https://doi.org/10.1016/S0967-0645(02)00193-5

You, Y. (2003). Implications of cabbeling on the formation and transformation mechanism of North Pacific Intermediate Water. *Journal of Geophysical Research*, *108*(C5), 3134. https://doi.org/10.1029/2001JC001285

Zahn, R., Pedersen, T. F., Bornhold, B. D., & Mix, A. C. (1991). Water mass conversion in the glacial subarctic Pacific (54°N, 148°W): Physical constraints and the benthic-planktonic stable isotope record. *Paleoceanography*, *6*(5), 543–560. https://doi.org/10.1029/91PA01327